LASER-INDUCED FLUORESCENCE MEASUREMENTS OF DUAL PLUMES AND COMPARISON OF LASER-INDUCED FLUORESCENCE AND CONDUCTIVITY PROBE MEASUREMENTS

A Thesis
Presented to
The Academic Faculty

by

Joseph C. Chrzan

In Partial Fulfillment
of the Requirements for the Degree
M.S. Civil Engineering in the
School of Civil and Environmental Engineering

Georgia Institute of Technology
August 2012

LASER-INDUCED FLUORESCENCE MEASUREMENTS OF DUAL PLUMES AND COMPARISON OF LASER-INDUCED FLUORESCENCE AND CONDUCTIVITY PROBE MEASUREMENTS

Approved by:

Professor Donald Webster, Advisor
School of Civil and Environmental Engineering
Georgia Institute of Technology

Professor Philip Roberts
School of Civil and Environmental Engineering
Georgia Institute of Technology

Professor Marc Weissburg
School of Biology
Georgia Institute of Technology

Date Approved: 29 June 2012

ACKNOWLEDGEMENTS

I am most gracious to my advisor Dr. Don Webster. He never pushed me where I could not go but he always kept me on track and was always able to answer all of my questions and help with every single one of my requests.

I would also like to thank David Murphy and Aaron True who were invaluable throughout my entire time here. They were always willing to help when I needed it most and never said no.

A special thanks goes to Dr. Philip Roberts and Dr. Marc Weissburg for agreeing to review this gem of a thesis.

TABLE OF CONTENTS

LIST OF TABLES

LIST OF FIGURES

SUMMARY

The planar laser-induced fluorescence (PLIF) technique is used in two different experiments. The first utilizes a single-color PLIF setup to compare PLIF measurements of rhodamine 6G concentration with probe measurements of salt concentration in a plume. The plume is created by an iso-kinetic release of the effluent into a turbulent open channel flow with a mean velocity of 5 cm/s. A total of 150 seconds of data recorded at 10 Hz is analyzed. These two sets of data should be comparable if normalized by the source solution concentrations of rhodamine 6G and salt, respectively. The second experiment employs a two-color PLIF setup to study the interaction of two different dye plumes of rhodamine 6G and oxazine 725 in a surrounding flow with the same characteristics as in the first experiment. Two nozzles are used at a cross-stream separation distance of 10 cm and release dye iso-kinetically into the surrounding flow.

The single-color PLIF results indicate that a separation distance of only 1 cm affects the two measurement results to the point where they are not comparable the majority of the time. However, several spikes in concentration are similar and a few have similar magnitude, but the conductivity probe measurements also seem to miss more spikes in concentration in comparison to the PLIF measurements. The different resulting concentrations may be attributed to three main factors. First, the instantaneous velocity at each time step is not used to determine the location of the area over which the PLIF concentration values should be averaged. The location of the x (streamwise) coordinates of the averaging rectangle should therefore be shifted according to the instantaneous velocity for every time step. Second, the stirring and distortion of the filaments of the dye/salt plume as it passes downstream can distort a

region of concentration in the x-y plane or even shift it out of the illuminated z plane, which may result in minimal to drastic differences since the filaments of the dye plume are rather large in comparison to the averaging area and probe sensor size. These two factors are the reasons for the differences in concentration values and the latter describes how spikes in concentration are sometimes either present or missing when compared with the other data set. The former, however, is only valid in describing the different magnitudes and not the differences in characteristics of the time series. More importantly, however, the plastic shielding around the conductivity probe acts as a barrier to proper comparison between PLIF and probe data and should have been removed. Because the shielding may affect the surrounding flow characteristics, it is the most likely culprit in assessing why the probe measurements were lower than the PLIF measurements.

Since the instantaneous measurements were not well correlated, the only comparable values would then be time-averaged. Therefore, the means, standard deviations, and maximum concentrations of the PLIF and conductivity probe concentration measurements are calculated and compared to one another. However, since it was originally hypothesized that instantaneous measurements between the two different methods would yield similar concentration values, a long time series was not collected. Additionally, the context of the experiement does not allow for long time series of measurements to be collected or analyzed. Because at least five minutes of data are required for statistical values to converge, the 50 seconds of measurements is not enough to properly compare the means and standard deviations. The mean concentration and standard deviation of the probe measurements are lower than their PLIF counterparts, albeit these values were not precise and only provide a very rough estimate of the true values. This is expected since there are fewer spikes in concentration in the conductivity probe values than in the PLIF values.

The two-color PLIF results demonstrate that dual plume measurements can be

performed in the context of plume tracking. The results show some interaction between the two dye plumes at several locations. It was found that turbulent stirring and molecular diffusion both act to sometimes result in overlap between rhodamine 6G and oxazine 725 filaments.

CHAPTER I

INTRODUCTION

Benthic crustaceans, such as blue crabs, utilize chemosensors to track odor plumes in order to find the source of distant food sources or mates (e.g., Weissburg and Zimmer-Faust 1994). They do this relatively quickly, so the use of the time-averaged concentration of these plumes is most likely not used since a very long time series is required for the mean concentration field to converge to any sort of useful information (Webster and Weissburg 2001). Rather, rapid fluctuations and small-scale variation in the odor plume are the most likely information employed by these animals in determining the source location of these foods or mates. In fact, rapid bursts at sufficiently high frequencies do induce behavioral changes (Page et al. 2010). Crabs sample sequentially, but not to exclusively detect concentration. However, sequential sampling is not used if the animal is moving quickly to track and orient itself as it moves closer to the source (Webster and Weissburg 2001).

Further, Webster et al. (2012) constructed an autonomous tracking agent which used three conductivity probes spaced to roughly correspond to the placement of a blue crab's chemosensors. They used this "robot" to track the source of a salt plume with a high success rate starting from far downstream. Instantaneous concentration measurements along with short time-averaged concentration data collected by the three probe sensors were used by the autonomous tracking algorithm to direct motion toward the plume source.

For the applications above, it is desirable to quantify the instantaneous concentration field of a turbulent plume in order to provide insight to the chemical signals

available to biological or robotic trackers. Measuring the instantaneous spatial distribution of the concentration field is challenging due to turbulent mixing creating an ephemeral and spatially complex filament structure. Laser-induced fluorescence is a optical technique that may be utilized to non-invasively measure the concentration of dye in water. A conductivity probe may also be useful in measuring concentration at a point, but the presence of the probe influences the surrounding flow.

The first objective of this thesis is to compare simultaneous PLIF measurements of dye concentration and conductivity probe measurements of salt concentration released together from the a point source. In this comparison, the PLIF measurements will be considered the "ground-truth", whereas the measurements of the conductivity probe will include the effects of local transport of molecules to the probe tip and temporal response of the sensor and other factors. The planar concentration field just upstream of a conductivity probe in the same plane of the conductivity probe tip was measured via LIF. The main point is to accurately average the concentration of dye in a small area just upstream of the probe tip and compare it to the probe tip measurement taken a very short time earlier. The advection velocity and separation distance are used to estimate the time delay between the respective measurements. The results of this comparison provide insight to the signals collected by the autonomous tracker described above.

The second objective is to develop a two-color PLIF system to measure the instantaneous concentration field of two overlapping plumes of different chemicals. The motivation is to quantify conflicting cues that may be presented to a tracking agent. For instance, the combination of attractive (i.e. food) and aversive (i.e., metabolites from injured blue crab) solutions have been used to examine blue crab chemosensory behavior (Moir and Weissburg 2009, Page et al. 2011a,b). In order to understand the tracking behavior of blue crabs or other crustaceans when presented with combinations of these cues, each plume structure must be quantified simultaneously.

The two-color PLIF system builds on previously reported systems (e.g., Soltys and Crimaldi 2011), and the system design is specifically tuned to address the plume tracking application.

CHAPTER II

LITERATURE REVIEW

This chapter provides a review of topics relevant to the thesis study. The primary emphasis is a review of turbulent plumes, the laser induced fluorescence (LIF) technique, and the experimental set up of previous LIF experiments.

2.1 Turbulent Plumes

A plume forms when chemicals are released from a point source in a moving fluid stream that transports the effluent in the downstream direction. They commonly occur in applications of point discharge of pollution or aqueous solutions. It is great of concern to know not only the basic characteristics of plumes but also how they are affected by and evolve in a turbulent environment. Fluctuations of certain characteristics such as concentration and temperature are of particular interest and behavioral characterization of these fluctuations is essential.

2.1.1 Mixing in Turbulence

Perhaps the most important initial concept of importance is mixing in a turbulent environment. By definition, turbulent mixing is the process by which a fluctuating turbulent flow dilutes and homogenizes certain quantities such as mass concentration, heat, and momentum (Webster, 2007). Two different processes must occur for turbulent mixing to take place, that relating to advection and that relating to diffusion. Because flow varies in space, regions of high concentration are advected away from neighboring regions and this process is known as turbulent stirring. This process results in regions of steep concentration gradients and irregularities in shape. An example of this is depicted in Figure 2.1. One can see from Figure 2.1 that the

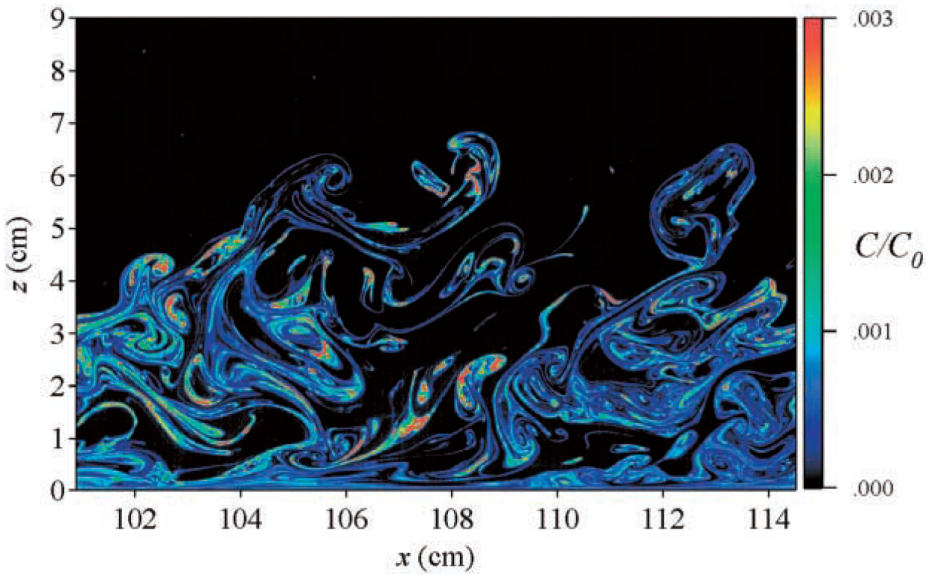

Figure 2.1: Instantaneous concentration field of a plume taken at its centerline (Crimaldi, 2001).

normalized concentration gradients of this planar laser induced fluorescence (PLIF) visualization and quantification are steep and that the turbulent stirring process is clearly depicted.

The other governing process is Fickian diffusion, in which concentration flux is proportional to the concentration gradient:

$$J = -D\frac{\partial \mathrm{C}}{\partial \mathrm{x}} \tag{2.1}$$

Diffusion acts to smooth the steep concentration gradients, diluting the volume of concentration and spreading it out into a larger volume. When coupled with turbulent stirring, diffusion may be quite effective at mixing concentrations of mass and takes considerably less time to mix when compared with molecular diffusion alone.

2.1.2 Length Scales of Turbulence

Length scales are commonly used to describe turbulent fields and these scales relate to the scales of concentration gradients described above as well as eddy sizes. These scales range from the size of the largest structures found within the flow to the size

of the smallest structures where eddies dissipate to heat. The integral length scale is an approximate measure of the largest eddies found within the flow and is usually assumed to be on the order of half of the flow depth.

The dissipation of turbulent kinetic energy to heat occurs at what is called the Kolmogorov microscale:

$$\eta = \left(\frac{\nu^3}{\epsilon}\right)^{1/4} \tag{2.2}$$

where ν is the kinematic viscosity of the fluid and ϵ is the dissipation rate of the turbulent kinetic energy. This microscale is not exact but rather an approximation of the smallest eddy sizes.

As stated above, molecular diffusion acts to smooth the steep concentration gradients at a small length scale. The scale at which this occurs is referred to as the Batchelor length scale:

$$L_B \approx \left(\frac{\nu D^2}{\epsilon}\right)^{1/4} \tag{2.3}$$

in which D is the molecular diffusivity of the substance being stirred in the flow. The Kolmogorov and Batchelor length scales are related:

$$\frac{\eta}{L_B} \approx Sc^{1/2} \tag{2.4}$$

where the Schmidt number, Sc, is defined as $\frac{\nu}{D}$.

2.1.3 Passive Scalars

In the application present in this experiment a nonreactive dye is used as the plume effluent. The dye plume may be described as a passive scalar plume in which flow dynamics are not affected due to the presence of the dye in such low concentrations.

It is of great interest to be able to describe how these passive scalars are transported as well as how they mix, so finding the spatiotemporal evolution of variance

and flux of these scalars is the primary interest. Boundary conditions must be accounted for because the flux and variance of the scalars are dependent upon them. It would be much easier to quantify and solve for these quantities if the small-scale behavior was independent from the large-scale behavior. Unfortunately, this is only the case with large Reynolds and Peclt numbers, so separation is almost never possible. At the small scale, behavior becomes more interesting and departs from the traditional Gaussian behavior proposed by original cascade theory. Fluctuations become skewed and intermittent and are extremely important in describing the turbulent mixing that occurs at this scale.

The convection-diffusion equation governs the dynamics of a passive scalar field (Dasi 2004):

$$\frac{\partial \Theta}{\partial t} + U_j \frac{\partial \Theta}{\partial x_j} = D\nabla^2 \Theta \tag{2.5}$$

in which D is the diffusivity of the tracer and U_j is the velocity where j=1, 2, 3 are the components in the x, y, and z directions. Θ represents the magnitude of any passive scalar. Common examples are concentration of chemical tracer (as in our case) or temperature. However, we will write Equation 2.5 in a slightly different format more specific to the case in which we are interested as:

$$\frac{\partial \tilde{c}}{\partial t} + \tilde{u}_i \frac{\partial \tilde{c}}{\partial x_i} = D\frac{\partial^2 \tilde{c}}{\partial x_i \partial x_i} \tag{2.6}$$

where $\tilde{c}$ is the instantaneous concentration and $\tilde{u}_i$ is the instantaneous velocity.

To solve for the concentration of Equation 2.6, the case in which a small bit of tracer or contaminant centered about a moving point is considered by changing to Lagrangian coordinates by converting Equation 2.6 to:

$$\frac{\partial \tilde{c}}{\partial t} + \frac{\partial}{\partial \zeta_i}\left[\tilde{c}\left(\tilde{u}_i\left(\zeta\right) - \tilde{u}_i\left(0\right)\right)\right] = \mathrm{D}\frac{\partial^2 \tilde{c}}{\partial \zeta_i \partial \zeta_i} \tag{2.7}$$

in which ζ is the difference between the Eulerian and Lagrangian point positions. The Eulerian velocity becomes $u\left(\zeta\right) - u\left(0\right)$. With a tracer volume smaller than the

Kolmogorov microscale, a linear velocity distribution may be assumed such that:

$$\tilde{u}_i(\zeta) - \tilde{u}_i(0) = \zeta_j \frac{\partial \tilde{u}_i}{\partial \zeta_j}(0) \tag{2.8}$$

and so the concentration evolution becomes:

$$\frac{\partial \tilde{c}}{\partial t} + \frac{\partial \tilde{u}_i}{\partial \zeta_j}\zeta_j \frac{\partial \tilde{c}}{\partial \zeta_i} = D \frac{\partial^2 \tilde{c}}{\partial \zeta_i \partial \zeta_i} \tag{2.9}$$

Molecular diffusion quickly homogenizes concentrations at small scales and the time scale for this to occur is on the order of $\sqrt{v/\epsilon}$, whereas the time scale of the large eddies (l/u) is much longer. The instantaneous concentration may then be decomposed into a mean concentration plus a concentration fluctuation and the transport equation becomes:

$$\frac{\partial C}{\partial t} + \frac{\partial}{\partial x_i}\overline{cu_i} = D \frac{\partial^2 C}{\partial x_i \partial x_i} \tag{2.10}$$

where C is the mean concentration and c is the concentration fluctuation. Often molecular diffusion on the mean concentration distribution may be neglected because turbulent diffusion increases the characteristic length scale of mean concentration gradients very quickly so that the ratio of the LHS transport term to the molecular diffusion term on the RHS becomes large.

Decomposing the scalar and velocity fields into mean and fluctuating components allows for the determination of scalar variance (θ^2), flux (θu_j) and dissipation rate (ϵ_θ), which in turn requires analysis of the statistics to understand how the passive scalar evolves. KOC theory showed that a cascade to small scales occurs at large Reynolds and Peclet numbers, after which the scalar field should become isotropic. This spectrum is predicted and may be represented as:

$$F_\theta(k_1) = C_\theta \epsilon^{-1/3} \epsilon_\theta {k_1}^{-5/3} \tag{2.11}$$

where the scalar variance (θ^2) is thereby:

$$\theta^2 = \int_0^\infty F_\theta(k_1)\, \mathrm{d}k_1 \tag{2.12}$$

with k_1 being the longitudinal wave number and C_θ being a universal constant. The power spectrum for the velocity fluctuations is described in similar terms as:

$$F\left(k_1\right) = C\epsilon^{2/3}{k_1}^{-5/3} \tag{2.13}$$

where C is a different constant. The above equation is what is commonly referred to as Kolmogorov's $k^{-5/3}$ law and experiments have shown C to be approximately equal to 1.5. However, strong variability in dissipation and mixing rates at this scale induces strong intermittency and KOC theory becomes insufficient for describing the scalar behavior.

2.1.4 Analytical Solution for a Point Source

A plume may be modeled as a continuous point source with mass flow rate $\dot{m}$, which yields a spatially-varying concentration field:

$$C\left(x, y, z\right) = \frac{\dot{m}}{4\pi Dx}\exp\left[\frac{-\left(y^2+z^2\right)u}{4Dx}\right] \tag{2.14}$$

where D is the diffusion coefficient, x is the distance downstream in the flow direction, u is the flow velocity, and y and z values determine the variation along the x-axis. This analytical model assumes that flow is strictly in the x direction, or that it has only a u component of velocity. Additionally, diffusion in the x direction is neglected ($D\frac{\partial^2 C}{\partial x^2}$ must be very small) for this model to be applicable. This latter assumption is not valid right at the source but only for $x \gg \frac{2D}{u}$.

The width of the cloud or plume may be approximated as four times the standard deviation:

$$w = 4\sqrt{2Dx/u} \tag{2.15}$$

Thus, assuming a steady velocity in the x-direction, the plume spreads linearly with x, the distance downstream from the point source. However, this model has severe restrictions and is only applicable in the laminar flow regime.

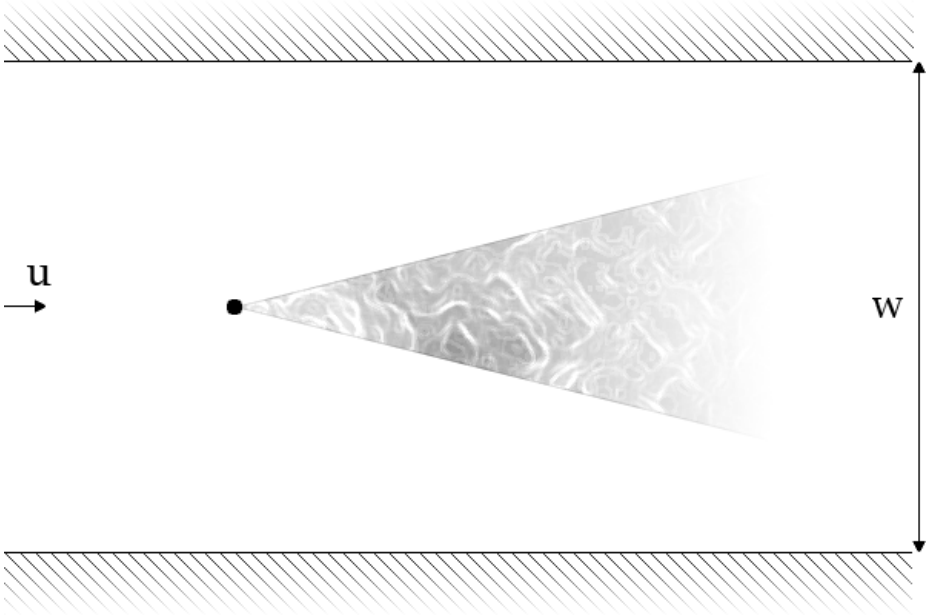

Figure 2.2: Ideal flume channel characteristics with iso-kinetic release of tracer.

2.1.5 Turbulent Properties of an Ideal Channel

To describe a plume beyond the laminar regime much more information must be taken into account since turbulence adds unpredictable and random characteristics to the flow. For the simplest case of an ideal rectangular channel with steady flow velocity u, channel width w, flow depth y, and tracer released at the center of the flume (see Figure 2.2),

the velocity profile near the bed may be described in terms of three separate and distinct regions: the viscous sublayer (nearest the wall), the logarithmic region or inertial sublayer, and the wake region or outer layer. The latter constitutes the majority of the flow depth with y/δ greater than about 0.2 and $U_\infty - U$ scaling with the wall friction velocity as:

$$\frac{U - U_\infty}{u^*} = \frac{1}{\kappa}\ln\frac{y}{\delta} + 2.5 \tag{2.16}$$

where u^* is the wall shear velocity defined in terms of the wall shear stress and density

as:

$$u^* = \sqrt{\frac{\tau_w}{\rho}} \tag{2.17}$$

and has units of velocity but no real physical meaning. The inertial sublayer is usually fitted with the following velocity profile:

$$\frac{u}{u^*} = \frac{1}{\kappa}\ln\frac{yu^*}{\nu} + A \tag{2.18}$$

Nezu and Rodi (1986) found that $\kappa \approx 0.412$ and $A \approx 5.29$ for smooth open channel flow. The thickness of the viscous sublayer may be found in terms of ν and u^* as:

$$\delta' \approx \frac{5\nu}{u^*} \tag{2.19}$$

and the velocity profile in the viscous sublayer is simply:

$$\frac{U}{u^*} = \frac{u^* y}{\nu} \tag{2.20}$$

Collectively, the viscous sublayer and these log profiles are known as the "Law of the Wall" and describe the mean velocity variation with distance from the bed for a turbulent flow.

Manning's equations has also been used to determine u^* in terms of the Manning number n, average velocity $\overline{u}$, and the hydraulic radius R_h of the channel as:

$$u^* = 3.8n\overline{u}R_h^{-1/6}[\text{ft, s}] \tag{2.21}$$

$$u^* = 3.1n\overline{u}R_h^{-1/6}[\text{m, s}] \tag{2.22}$$

with the hydraulic radius defined as A/P, or the area over the wetted perimeter.

2.1.5.1 Reynolds Stress Variation Near the Bed

In our case with turbulent flow in an idealized flume, the Reynolds stresses are zero at the bed and reach a maximum a short distance away then return to zero as distance increases toward the free stream. $\overline{u^2}$ becomes the largest normal stress because energy is fed into the longitudinal normal stress from the mean flow via shear production whereby energy is then distributed to the other components.

2.1.6 Instantaneous Concentration Field of a Plume

Crimaldi et al. (2002) detailed the mean and instantaneous characteristics of a turbulent passive scalar plume. They found that at any given moment in time every plume has certain instantaneous characteristics. The most obvious of which is the very filamentous nature of the substance being released. Instead of diffusing as the plume evolves downstream, the filaments stretch and move due to the turbulent flow. Dye concentration is high within these filaments and the concentration outside of the filaments is close to zero. Filaments also appear to come in bursts as they travel downstream and lateral motions spread the substance away from the centerline. Shear and turbulence act to smear the well-defined structures to lower concentrations as the substance moves downstream, and the scalar structures depend on the momentum field and the streamwise distance from the source.

Rahman (2002) describes the importance of quantifying the fluctuations in concentration. It is essential in determining and predicting environmental and health effects due to hazardous pollution. Bed roughness also plays a major role in the turbulent transport of an effluent in a flow. Bed roughness acts to decrease concentration fluctuations and does so more quickly the rougher the bed. As such, the concentration PDF becomes Gaussian more quickly as the downstream distance increases.

2.1.7 Time-averaged Concentration Characteristics of a Plume

Mean concentrations of a plume have two main characteristics of which are a Gaussian distribution and self-similarity of the time-averaged concentration field about the plume centerline (c_{cl}). The mean plume structure in the streamwise direction varies gradually in comparison to structural variations in the cross-stream or transverse (y-z) plane, thus literature typically reports information in this plane most often. Webster et al. (2003) detailed the LIF measurements of a turbulent plume and found the above characteristics to be accurate. They compared the experimental results with

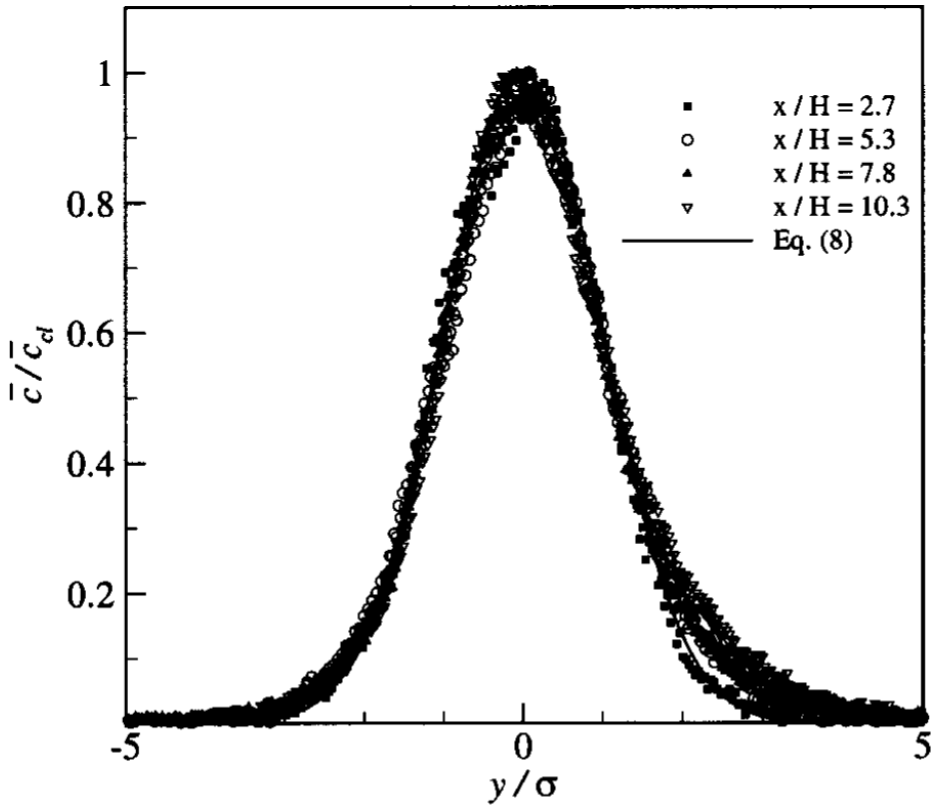

Figure 2.3: Comparison between time-averaged normalized concentration and Gaussian profile with σ calculated from a linear regression of $\ln(\bar{c}/\bar{c_{cl}})$ and y^2 (Webster et al., 2003).

a Gaussian profile and found both to agree very well with one another as shown in Figure 2.3. Rahman and Webster (2005) and Webster and Weissburg (2001) both had very similar results, and in fact all literature reports the same characteristic results.

Variance in the mean structure increases as the distance from the center of the plume radiates outward since the turbulent plume contains the bulk of its higher concentration around the plume centerline with filaments traveling sporadically further away from the centerline. Webster et al. (2003) showed that the variance follows a similar reasoning in the streamwise direction, whereby the variance is stronger closer to the source and decays exponentially until $x/H = 2$ where the decay then becomes more gradual and follows a power-law. In the later regime ($x/H = 2$) the plume becomes homogeneous faster than it dilutes.

Closer to the center of the plume the presence of non-zero concentration occurs the most and as such has a higher intermittency than areas further away, which have lower intermittency (or are more sporadic). Higher intermittency also requires a longer time series in order to resolve proper statistical data.

Fackrell and Robins (1981) found that the majority of fluctuations in concentration occur close to the source and that these fluctuations become less common as dye is advected and dissipated downstream. It was also determined that flux did not depend on the size of the dye source. Vertical flux was self-similar and lateral flux followed Gaussian profiles.

2.1.8 Concluding Remarks To Turbulent Plumes

Although complicated and variable, turbulence and turbulent plumes clearly have certain common characteristics that describe how the flow may behave and how concentrations of a tracer or effluent may be affected. Different measurement techniques have been used but the most commonly used technique has been and continues to be laser-induced fluorescence due to its noninvasive application and ease of use, although much of the equipment can be very expensive and sometimes dangerous if safety precautions are not properly followed. The information gleaned from LIF measurements may be directly related to the variables of interest presented in the preceding section and therefore a complete description of many major aspects of turbulent plume evolution is possible.

2.2 Review of Laser-Induced Fluorescence (LIF) Technique

Quantitative flow visualization techniques that use soluble dyes is of great interest in many fields of study for a variety of reasons. Laser-induced fluorescence (LIF) is one of the most commonly used techniques that accomplishes this quantification and visualization. The purpose of this section is to review the historical development of LIF.

Osborne Reynolds is perhaps the most renowned experimentalist who pioneered the use of dyes for visualizing flow, as evident in his laminar and turbulent pipe flow experiments during the late nineteenth century. Quantitative dye evolution did not come until much later, when laser-induced fluorescence was first used in experiments performed by Nichols et al. (1972), Owen (1977), and Liu et al. (1977) during the mid-1970s (Dickman 2008). Dimotakis and Koochesfahani (1985, 1986) published several seminal LIF studies in the mid-1980s which provided a basis for modern LIF use. The technique has continued to be refined and developed in subsequent years. For example, Walker (1987) proposed the need to consider temperature and pH variation when doing any measurements because fluorescence from the dye may vary, depending on the type of dye used, as the temperature and pH change. Walker (1987) also gives a very well-detailed description of the principles of LIF and how to properly set up an experiment. Ferrier et al. (1993) detailed the steps and corrections needed to extract accurate concentrations from the measurements taken.

2.2.1 Fluorescence

A fluorescent molecule is defined as a molecule that absorbs light in a certain range of wavelengths and emits light at a different wavelength. First, it becomes excited when the incoming light is absorbed. An outer electron will jump from the ground state to the excited singlet or triplet state. Once there, it may return to its ground state rapidly or slowly. The rapid return may happen in one of two ways; first, it may simply return from the singlet state via radiationless collision, or it may fluoresce at a certain wavelength, as shown in Figure 2.4, depending on the molecule or tracer used. A slow return from the triplet state results in phosphorescence whereby the absorbed radiation may be delayed and re-emitted at a lower intensity.

The emitted wavelength is longer than the absorbed wavelength because fluorescence occurs at the lowest vibrational level in the singlet state. The fluorescence

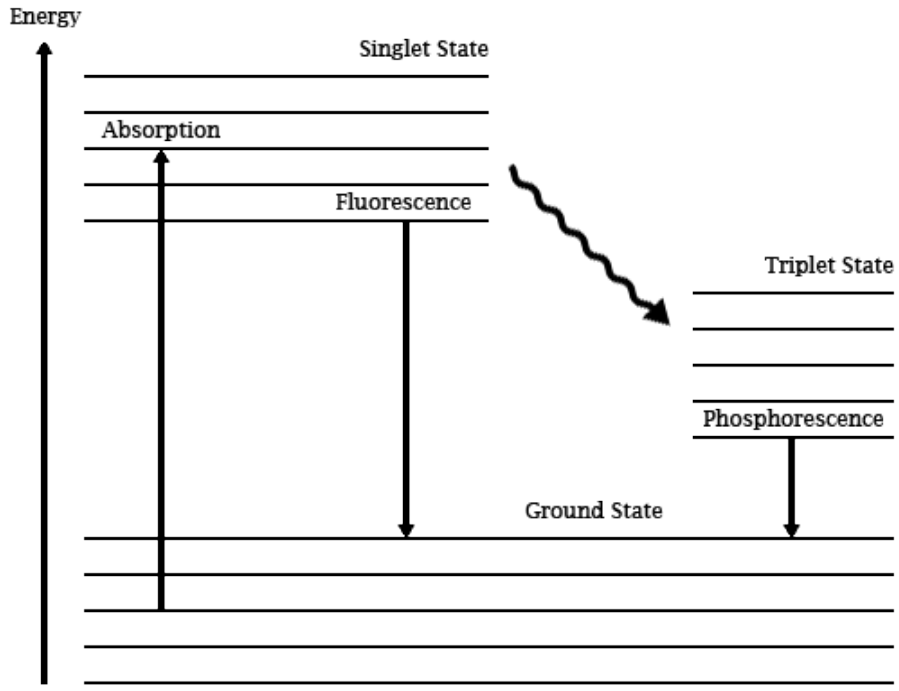

Figure 2.4: Diagram illustrating the possible modes of an excited electron.

process varies in the amount of time it takes to complete, but generally it is very brief. For example, a common tracer such as fluorescein takes 5 ns to fluoresce. It is important to note that the fluorescence is randomly polarized and the intensity is independent of direction.

2.2.2 Types of LIF

LIF is versatile and may be used one-dimensionally, two-dimensionally, or in three dimensions. It is most commonly used to measure a planar cross-section of a concentration field (2D). This type of LIF is widely known as PLIF (planar laser-induced fluorescence) and the acronym is often used interchangeably with LIF since it is so common (Crimaldi 2008). However, more recently 3D LIF , which is an extension of PLIF, has been used to obtain volume concentration fields (Dahm et al. 1991 , Tian and Roberts 2003 , Dickman et al. 2009). Regardless of dimensionality, all types of LIF follow the same procedure in determining the concentration of interest.

2.2.3 Theoretical Background

This section describes the mathematical background of the LIF technique, specifically the equations needed to quantify concentration. The material in this section largely follows that in Crimaldi (2008). As an initial relationship, fluorescence is directly related to concentration and excitation intensity via the following:

$$F \propto \frac{I}{1 + I/I_{sat}} C \tag{2.23}$$

with I_{sat} being the saturation intensity of the particular tracer or dye used. Typically, excitation is weak, meaning $I_{\text{sat}} \ll I$ for most LIF experiments, so the equation may be reduced to:

$$F \propto IC \tag{2.24}$$

which may seem like a straightforward determination for concentration, but I is rarely known and is not independently measured. Also, intensity may vary temporally and spatially. To account for this intensity variation, the Beer-Lambert law is used to describe the change in intensity in relation to concentration in space:

$$\frac{dI}{I} = -\epsilon C \mathrm{d}r \tag{2.25}$$

with ϵ being an extinction coefficient. Hence, the intensity of a ray of light passing a small distance through a concentration field is:

$$I\left(r_1\right) = I\left(r_0\right) \exp\left[-\epsilon \int_{r_0}^{r_1} C\left(r\right)\, \mathrm{d}r\right] \tag{2.26}$$

Attenuation may be neglected if:

$$\epsilon \int_{r_0}^{r_1} C\left(r\right)\, \mathrm{d}r \ll 1 \tag{2.27}$$

If the concentration field is uniform, Equation 2.27 may be reduced to:

$$\epsilon \left(r_1 - r_0\right) C \ll 1 \tag{2.28}$$

Systems that follow Equation 2.27 are termed "optically thin".

Quantum efficiency is the ratio of light energy emitted to energy absorbed and is given the symbol ϕ. Utilizing quantum efficiency, Equation 2.24 may be stated as:

$$\mathrm{d}F = \phi \epsilon I C \mathrm{d}V \tag{2.29}$$

for omnidirectional fluorescence along a ray path.

In PLIF applications, a general form of the laser intensity distribution may be written as:

$$I\left(r,\theta,z\right) = Pa\left(r,\theta\right) f\left(r\right) g\left(\theta\right) h\left(z\right) \tag{2.30}$$

with P being the power of the laser beam and a being the attenuation due to dye absorption defined as:

$$a\left(r,\theta\right) = \exp\left[-\epsilon \int_0^r C\left(r',\theta\right)\, \mathrm{d}r'\right] \tag{2.31}$$

If there is no attenuation Equation 2.30 may be reduced to:

$$I\left(r,\theta,z\right) = f\left(r\right) g\left(\theta\right) h\left(z\right) \tag{2.32}$$

with no reliance on laser beam power or attenuation. The functions $g(\theta)$ and $h(z)$ depend on the beam shape and how the optics form a laser sheet. They vary from 0 to 1 with the maximum occurring over the entire range of the respective θ and z scales of the sheet formation. Combining Equations 2.29 and 2.30, the total fluorescence may be obtained via integration as:

$$F = \phi \epsilon P a\left(r,\theta\right) f\left(r\right) g\left(\theta\right) C \Delta A \tag{2.33}$$

Where C is the averaged concentration over a small imaged volume ΔV. If it is assumed that reabsorption of fluoresced light by the dye is negligible, then the imaged fluorescence intensity at any pixel location in an image is:

$$I_F\left(i,j\right) = \beta\left(i,j\right) \frac{F}{\Delta A} = \alpha\left(i,j\right) a\left(r,\theta\right) C \tag{2.34}$$

with β being the fraction of the omnidirectional fluorescence actually received by the camera. α is merely a coefficient encompassing all concentration independent constants that has dimensions of intensity per concentration. Equation 2.34 may then be rearranged to find an expression for the concentration:

$$C = \left[\alpha\left(i,j\right)a\left(r,\theta\right)\right]^{-1} I_F \tag{2.35}$$

with α being empirically determined via image correction and a being numerically integrated for each image according to the instantaneous concentration field. Additionally, total fluorescence may be reduced to the following:

$$F\left(r_1\right) = I\left(r_0\right)\phi\epsilon C\exp\left(-\epsilon r C\right) \tag{2.36}$$

only if the concentration is uniform. Equation 2.36 is then useful to determine the value of ϵ for a particular dye or tracer for any given uniform concentration.

2.3 Setup of LIF Experiments

There are several key elements to a proper LIF experimental setup. These include lasers, fluorescent dyes, sheet optics, and cameras. The laser emits a beam at a certain wavelength. Sheet optics spread the beam into a flat plane and directs the light towards the area of interest. The dye in the flow must be chosen carefully to absorb light corresponding to the laser wavelength. The dye then excites and emits light at a different wavelength. A camera, fitted with a filter that only allows for light in the excitation wavelength to pass through, captures images of the emitted light field.

2.3.1 Lasers

The majority of LIF experiments performed and reported in literature have used an Argon ion laser at either 488 or 514.5 nm wavelengths with continuous emission. The other most common laser is known as the Nd:YAG laser, which is a pulsed type

operating at 532 nm (frequency-doubled). Other laser types have been used in many experiments, but comparison of these two most common types is beneficial.

Ion lasers have superior beam quality, continuous output, produce a beam that has a nearly Gaussian-distributed cross-section, and when operated properly have a stable power output which simplifies the calibration procedure for the system. Nd:YAG lasers are able to pulse a beam at least six orders of magnitude higher than ion lasers. Because of this, the energy captured per image exposure using a Nd:YAG laser is much higher. However, beam quality is often inferior and the power output, and hence the distribution across the beam cross-section, may vary from pulse to pulse. In addition, the high power output can cause problems if the laser excitation intensity is not small in relation to the dye saturation intensity, thus violating the weak excitation assumption introduced by Equation 2.24.

However, if the system is optically thin, then accurate PLIF measurements may still be taken because dye absorption does not result in intensity variations, so the nonlinear relationship between F and I does not matter under such conditions. Additionally, fluorescence and concentration have a linear relationship for many of the most common dyes including fluorescein, rhodamine WT, and rhodamine 6G, making system calibration easier.

2.3.1.1 Fluorescent Dyes

A necessary component of LIF is the dye. Choosing a proper dye that is compatible with the laser being used is an essential step in properly conducting an LIF analysis. Suitability of a dye is based on an absorption spectrum that is compatible with the laser excitation wavelength, large separation between absorption and excitation spectra, and high quantum efficiency so that signal strength is maximized. As indicated by Walker (1987) and others, sensitivity to temperature and pH is dye specific, so these must also be carefully considered. In addition, susceptibility to photobleaching

and linearity between fluorescence and concentration also need to be considered.

Choice of dye is limited to water soluble dyes if the experiment is being conducted in aqueous flow. Fluorescein, rhodamine WT, and rhodamine 6G are xanthene-class dyes that are water soluble with large quantum efficiencies (over 95%). Of these three dyes, fluorescein is most commonly used due to its peak absorption at a wavelength of 490 nm. A common Argon ion laser may emit at a wavelength of 488 nm, making for a very close match. Additionally, the dye fluoresces at 510 nm, offering good separation between excitation and emission wavelengths and it also has low sensitivity to temperature variations. However, the absorption spectrum of fluorescein is particularly dependent upon pH, resulting in negligible absorption below a pH level of approximately 4. It is also susceptible to photobleaching, but typically this is minimized in most PLIF experiments. Walker (1985) altered the pH levels by using two different acids and bases, ammonium hydroxide in boric acid and citric acid in sodium hydroxide. Intensities were then obtained at differing pH levels as shown in Figure 2.5.

Photobleaching is a process by which a fluorescent molecule loses the ability to fluoresce due to exposure to laser light (Crimaldi 1997). This may result in a reduced response to an increase in laser intensity or dye concentration, so the process should always be carefully considered. The different processes behind photobleaching still remain a mystery; however, Crimaldi (1997) described a way to quantify normalized concentration and fluorescence as a function of a photobleaching parameter, B as shown in Equations 2.37, 2.38, and 2.39:

$$C^* = \exp\left\{-B\left[1+\operatorname{erf}\left(\sqrt{2}x^*\right)\right]\exp\left[-2\left(y^{*2}+z^{*2}\right)\right]\right\} \tag{2.37}$$

where B is defined in terms of P, the laser power, Q_b, the quantum bleaching efficiency, σ, the absorption cross-section, h, Planck's constant, v, the frequency of the

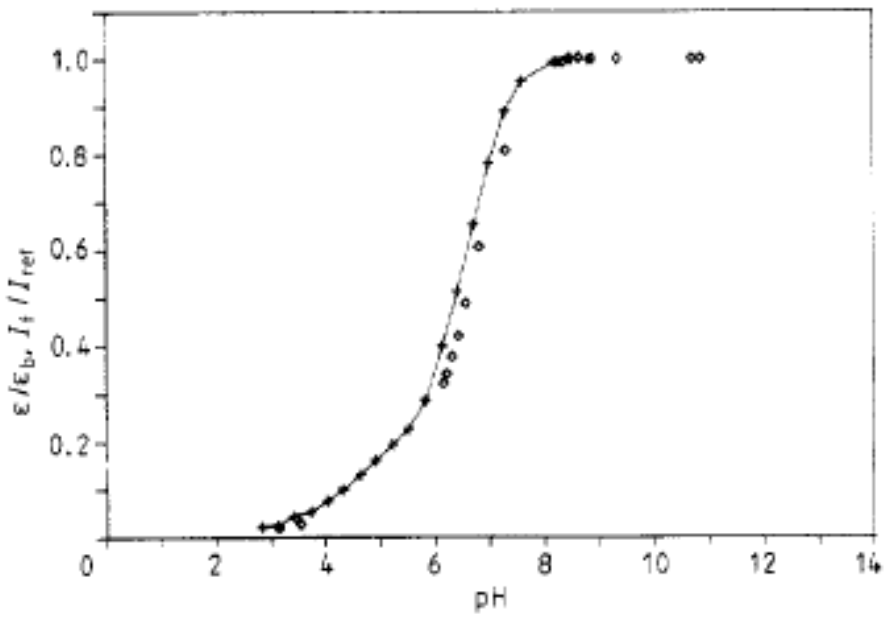

Figure 2.5: Variation of intensity with pH for fluorescein. + indicates extinction measurements by Lindqvist (1960). ◇ indicates fluorescence intensity measurements by Walker (1986).

excitation source, and U, the fluid velocity as:

$$B = \frac{PQ_b\sigma}{\sqrt{2\pi}ahvU} \tag{2.38}$$

and using Equation 2.24 at the origin of the control volume :

$$F^* = I^*C^* = \frac{2\sqrt{2}}{\pi^{3/2}}\exp(-B) \tag{2.39}$$

A plot of F^* as a function of B is located in Figure 2.6 where the line represents the equation for F^*. The dye data tested match almost perfectly with the equation. The results clearly show that photobleaching is a necessary consideration and cannot be ignored if velocity is not taken into consideration. However, there is a relationship between F^*, B, and U (the flow velocity) such that:

$$\frac{\partial F^*}{\partial U} = \frac{2\sqrt{2}}{\pi^{3/2}U}B\exp(-B) \tag{2.40}$$

and from Equation 2.40 it may be determined that as U increases B must decrease, meaning that as long as the flow velocity is sufficiently high enough photobleaching

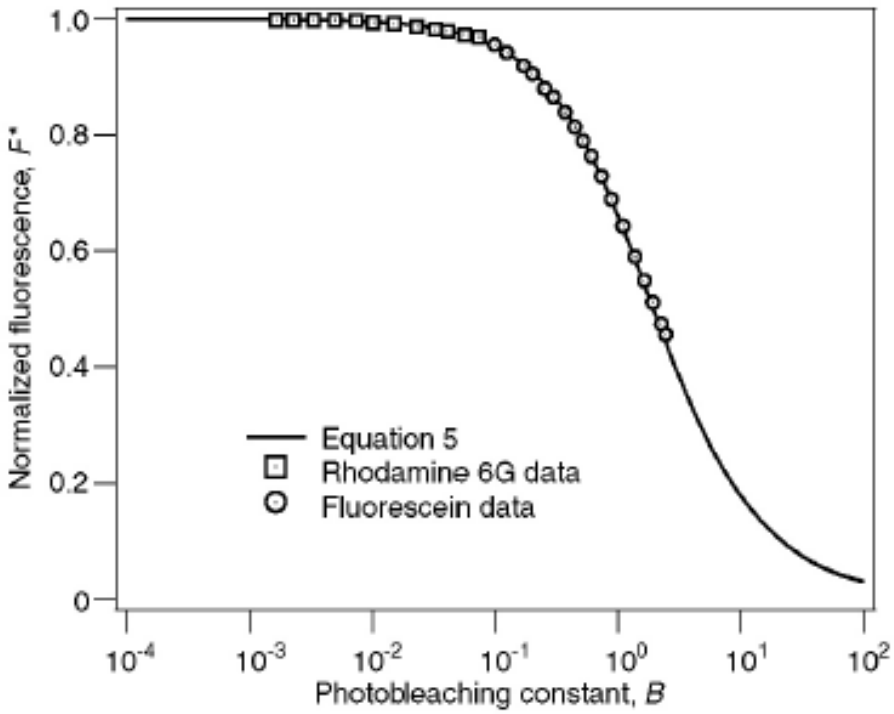

Figure 2.6: Normalized fluorescence as a function of photobleaching parameter, B (Crimaldi 1997).

effects may actually be discounted. However, the experimentalist should always make sure that this is the case so that accurate measurements of intensity may be made. If flow velocity in a particular experiment is low enough such that photobleaching affects measurements of intensity, corrections are possible and are detailed in the corresponding image correction section.

Rhodamine 6G and rhodamine b are also popular dye choices and have peak absorptions near 525 nm and 555nm and peak emissions near 560 nm and 580 nm, respectively. Rhodamine 6G is very resistant to photobleaching; however, there is little temperature and pH dependence data available. Rhodamine b is insensitive to pH differences but not temperature. This property of the dye may be utilized to measure temperature using PLIF. Unfortunately, Rhodamine b can have negative health effects if it comes in contact with the human body.

To take advantage of the useful properties while minimizing negative effects, more

recently synthetic dyes have been created and used in some aqueous PLIF experiments. They are brighter, more resistant to photobleaching, and less pH sensitive. The only disadvantage is that they are more expensive.

2.3.2 Sheet Optics

Optics are needed to transform the laser beam into a sheet if a concentration field is to be measured. A lens or scanning mirror is typically used to form the sheet. The lens will spread the laser beam out into a plane whereas the scanning mirror will rapidly rotate back and forth to create a similar sheet of laser light. However, because there is flow which is moving through the laser sheet, and consequently the imaging area, the images will be distorted. This distortion is related to the ratio of the image integration time to an advective timescale and it depends on whether a lens or a scanning mirror is used to create the sheet of light. If a lens is used, the laser sheet is static; however if a scanning mirror is used, it is called a dynamic scan.

To minimize this distortion evident in the fixed lens case a constraint may be imposed such that:

$$\Re_1 = \frac{\delta}{\lambda_s} \ll 1 \tag{2.41}$$

where λ_s is a length scale for local scalar features and δ is the distance advected of these features during the laser scan. Figure 2.7 shows this phenomenon using plus symbols as the features of interest being distorted.

If the flow is completely in the horizontal direction as depicted, then δ is simply the width of the vertical components of the plus symbols if a lens was used to produce the laser sheet.

If dynamic scan was used then little to no blurring of the features occurs and the spatial difference between the actual feature pattern at t = 0 and the image captured will give the value of δ. Additionally, the separation distance between each plus appears to be reduced because the dynamic scan occurs in the opposite direction of

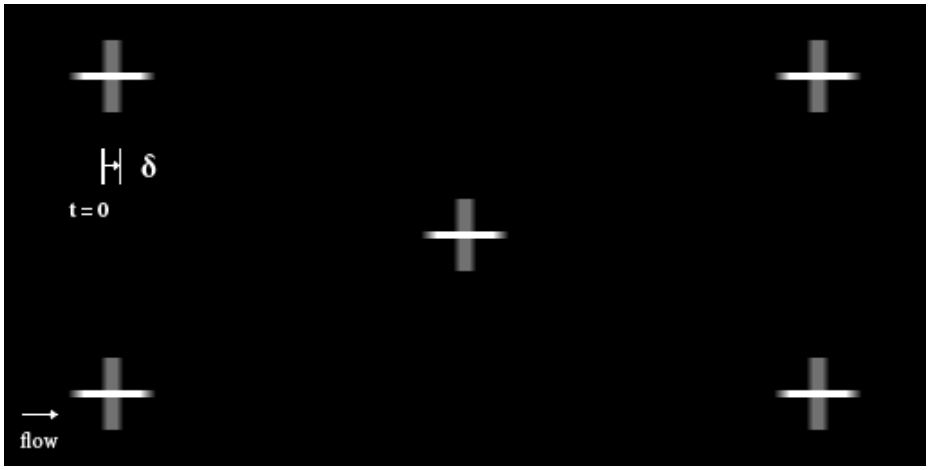

Figure 2.7: Simple example showing advective distortion of simplified features of an image.

advection. If the scan was in the direction of flow then the features would appear further apart. This distortion can be minimized by imposing the following restriction:

$$\Re_2 = \frac{\delta}{L} \ll 1 \tag{2.42}$$

where L is the length of the imaged area. Typically $\Re_2$ is two to three orders of magnitude less than 1.

Usually it is much easier to satisfy Equation 2.42 compared to Equation 2.41 so there is an advantage to performing a dynamic scan over using a sheet-forming lens. Since error is minimized more as scales are reduced, dynamic scan becomes more accurate and a better choice.

Before the laser beam arrives at the scanning mirror or sheet lens it is often preferred to focus the beam with a focusing lens. With the focal length, f, of the focusing lens and laser beam width, w_L, known the radius of the focused beam is a function of the horizontal distance, z, from the focal length given by:

$$w\left(z\right) = w_0 \left[1 + \left(\frac{\lambda z M^2}{\pi w_0^2}\right)^2\right]^{1/2} \tag{2.43}$$

as shown in Figure 2.8 below, where λ is the beam wavelength, w_0 is the beam radius at $z = 0$, and M^2 is beam quality where a value of 1 indicates an ideal Gaussian

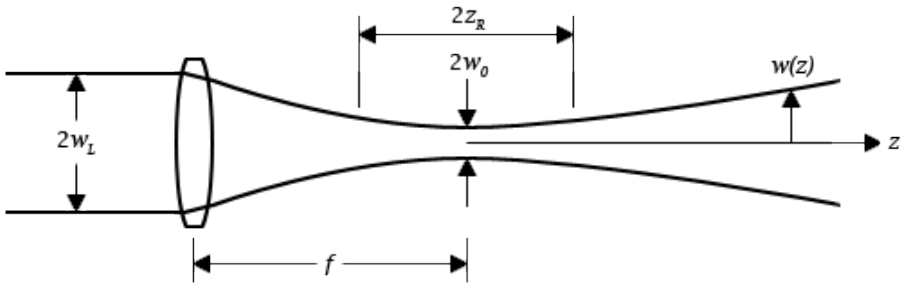

Figure 2.8: Geometry of a laser beam as it is focused by a focusing lens.

beam. Typical ion laser values range between 1.1 and 1.7 and higher energy lasers may have an M^2 larger than 10.

A beam diameter may be defined such that:

$$2w_0 = 2M^2 \frac{\lambda f}{\pi w_L} \tag{2.44}$$

Additionally, a beam expander may be used as to increase w_L, resulting in a decrease in w_0 given that the focal length remains constant, i.e. the same lens is used. A portion of the beam is kept approximately constant in size as w_L and w_0 change size and this section is known as the Raleigh length such that:

$$2z_R = 2\frac{\pi w_0^2}{\lambda} \tag{2.45}$$

and:

$$w\left(z_R\right) = \sqrt{2} w_0 \tag{2.46}$$

The beam expander should be located between the laser and focus lens in order to properly function. Finally, it is important to note that all beam measurements in the previous equations are results for the ideal case, so it is beneficial to simply measure the laser sheet thickness directly by image.

2.3.3 Cameras

Many advances have been made in the area of photography in recent years. With the rapid growth and improvements in technology cameras have become far better than their predecessors. Film cameras were originally used in early PLIF experiments with the majority of the work used for qualitative analysis. With the introduction of digital technology, CCD digital cameras began being used as early as 1990 and became the camera of choice. More recently, however, CMOS and sCMOS cameras have become popular and advantageous. Because a dye fluoresces in a very narrow band of wavelengths, higher performance grayscale cameras are typically preferred.

There are three key features or attributes of a digital camera: pixel count, bit depth, and frame rate. All are preferred to be maximized of course, but trade-offs between each exist. Earlier cameras had a resolution of 256 x 256 but now with the latest sCMOS technology, resolutions up to 2560 x 2160 are attainable and this number will certainly continue to increase. Bit depth determines the resolution of the intensity. Assuming a bit depth of N, 2N grayscales may be resolved. The latest technology allows for a bit depth of 16, or $2^{16} = 65{,}536$ grayscales. Frame rate determines how quickly successive images may be acquired. High-speed PLIF applications may use a frame rate of up to about 1000 frames per second, but typically anywhere between 30 and 100 fps is considered reasonable depending on the application. Finally, the sensitivity of the camera at the fluorescence wavelength controls the exposure time for the images.

Special lenses are often required for most PLIF applications. A flat-field lens is popular because it is designed for imaging planar surfaces. Typical lenses are spherical, so that the location of focused objects is on a radial arc from the sensor; thus flat-field lenses may allow for better uniform focal sharpness.

Additionally, an optical filter is used alongside the lens in order to allow only the fluoresced wavelength band to be imaged, blocking everything else out, especially the

damaging UV band.

2.3.4 Image Correction

Once the experiment is performed and raw images have been captured by the camera, they cannot simply be used for quantitative analysis of dye concentration; instead, they must be calibrated and corrected. Crimaldi (2008) provides an excellent extension of many previous image processing techniques used by other seminal papers, so that process will be followed closely.

The major key for calibration is to take a background image of a uniform, known concentration. From this background image, the collection of concentration-independent constants $\alpha(i,j)$ may be determined. For any image, the dye concentration may be decomposed into a uniform background concentration and a concentration structure that is above the background level:

$$C_n(i,j) = c_n(i,j) + b_n \tag{2.47}$$

From Equation 2.31 the attenuation coefficient may also be decomposed into two components due to c_n and b_n:

$$a(r,\theta) = a_c(r,\theta)\, a_b(r) \tag{2.48}$$

The intensity of the uniform background is calculated as:

$$B_n(i,j) = \alpha(i,j)\, a_b(r)\, b_n + D(i,j) \tag{2.49}$$

with $D(i,j)$ being the dark-response of the camera, acquired by taking an average of images with the lens cap in place, and the intensity in any n^{th} image may be calculated as:

$$I_n(i,j) = \alpha(i,j)\, a_c(r,\theta)\, a_b(r)\, [c_n(i,j) + b_n] + D(i,j) \tag{2.50}$$

Combining the background intensity equation and the latter equation, $c_n(i,j)$ may be determined as:

$$c_n(i,j) = \frac{b_n}{a_c(r,\theta)} \frac{I_n(i,j) - [a_c(r)\{B_n(i,j) - D(i,j)\} + D(i,j)]}{B_n(i,j) - D(i,j)} \tag{2.51}$$

If $I_n \ll B_n - D$ this equation may be reduced to:

$$c_n(i,j) \approx \frac{b_n}{a_c(r,\theta)} \frac{I_n(i,j) - B_n(i,j)}{B_n(i,j) - D(i,j)} \tag{2.52}$$

This equation allows for a direct calculation of concentration at any pixel in a particular image without the need to calculate α. First, imperfections such as variation in pixel sensitivity and optical distortions are corrected by the latter fraction of Equation 2.52, then the multiplication by b_n scales the image to dimensional units. Lastly, division by a_c corrects any attenuation that is present where a_c is calculated from Equation 2.31. To ensure $I_n \ll B_n - D$ is always true and that Equation 2.52 remains valid, a camera with a large bit depth should be chosen.

To calculate b_n an explicit dose calculation is typically performed by determination and use of a calibration curve. This curve may be constructed by taking different images for multiple known concentrations. Usually a certain amount of dye is mixed with a predetermined amount of water in a tank. An image is captured and the process is repeated for differing concentrations until a suitable calibration curve is attained.

Because the background image correction technique only corrects for errors that do not vary with time, additional corrections may be required to achieve accurate images. Most commonly, variations in laser power from image to image may be present, notably if a pulsed laser was used in the experiment. To correct for the power variation, a power meter may be used to measure the laser power for each image as the beam passes through a volume of known concentration. Once these PLIF image correction techniques are used and all errors are corrected for, all of the images will show accurate quantification of dye concentration fields.

Melton and Lipp (2003) offer several important recommendations when performing an experiment involving LIF with higher laser powers. The fluorescent dye should have a linear relationship between laser intensity and concentration. The experiment should also ensure optically thin conditions. More importantly, errors due to high intensity excitation should be compared with the accuracy and precision that the experiment requires.

Tokumaru and Dimotakis (1995) used LIF image results to calculate velocity fields. This method is an alternate to PIV (particle image velocimetry), although the latter is easier to perform. Series expansions of image displacement and a nonlinear correlation method were used to estimate fluid velocities and velocity gradients and vector fields were calculated. The method used works for both two-dimensional and three-dimensional sets of data and the accuracy of the velocity results may be improved by increasing the order of the series expansions.

2.4 Two-color LIF

There are two studies that used a two-color method that are of particular interest by Soltys and Crimaldi (2010) and Natrajan and Christensen (2008). Watanabe et al. (2007) also used a two-color LIF method to measure temperature but with higher powered pulsed lasers. The former used the technique to visualize the interactions between two parallel jets and the latter two were able to quantify temperature variation with fluorescence emission to within $0.5 \circ C$.

Soltys and Crimaldi (2010) used two independent single-color PLIF systems simultaneously which had negligible interference with one another. When performing two-color LIF, it is a requirement that the two lasers should have a large separation in beam wavelengths. In this case, an Argon ion laser was used with an emission wavelength of 488 nm along with a Krypton ion laser with an emission wavelength

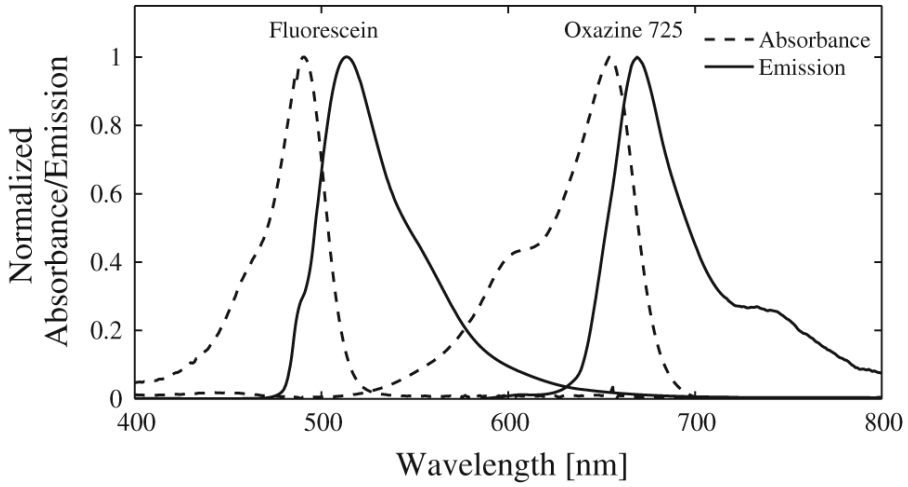

Figure 2.9: Absorption and emission spectra for fluorescein and oxazine 725 (Soltys and Crimaldi 2010).

of 647 nm, allowing for a large separation of emission wavelengths. Similarly, the two dyes must have separation in both absorption and emission spectra as to avoid interference with one another. To this end, fluorescein and oxazine 725 were chosen and as such, both spectra are distinctly separate in order to minimize crosstalk as shown in Figure 2.9.

It is clear that there will inevitably be at least some amount of crosstalk from Figure 2.9. This leads to what is referred to as Type I errors where fluoresced light from one system is detected by the other. Type II and Type III errors also may occur where fluoresced light by one dye is absorbed by the other. However, these Type II and III errors may be minimized by ensuring that the system is optically thin. Additionally, dyes must also be non-reactive. Two cameras were used with two different filters to each allow only the emitted fluorescein or oxazine 725 fluoresced light through. The system configuration used a dichroic mirror to co-align the laser beams before they reached the rotating mirror. Otherwise, most everything else followed the standard PLIF setup and procedure.

To account for the Type I error similar methods were used to Crimaldi (2008).

The pixel intensities in the background images for systems one and two are as follows:

$$B_{1,n} = \alpha_1 b_{1,n} + D_1 \tag{2.53}$$

$$B_{2,n} = \alpha_2 b_{2,n} + \alpha_1 \lambda b_{1,n} + D_2 \tag{2.54}$$

where λ accounts for crosstalk between systems and α represents a collection of concentration-independent constants. The fluorescence intensities are similarly:

$$I_{1,n} = \alpha_1 \left[C_{1,n} + b_{1,n}\right] + D_1 \tag{2.55}$$

$$I_{2,n} = \alpha_2 \left[C_{2,n} + b_{2,n}\right] + \alpha_1 \lambda \left[C_{1,n} + b_{1,n}\right] + D_1 \tag{2.56}$$

Combining the above equations, expressions for concentration without reference to α may be obtained as follows:

$$C_{1,n}(i,j) = b_{1,n} \frac{I_{1,n} - B_{1,n}}{B_{1,n} - D_1} \tag{2.57}$$

$$C_{2,n}(i,j) = b_{2,n} \frac{I_{2,n} - B_{2,n} - \lambda \left[I_{1,n} - B_{1,n}\right]}{B_{2,n} - D_2 - \lambda \left[B_{1,n} - D_1\right]} \tag{2.58}$$

λ varies and is based on camera spectral sensitivity, relative laser power, and the fluid pH. It may be calculated empirically along with b_1 and b_2 by imaging a tank with different known concentrations of both dyes, similar to how intensities are calibrated in a single-color LIF system. Following this process eliminates the concern for crosstalk and thus proper images may be calibrated and obtained.

Natrajan and Christensen (2008) utilized two-color LIF to measure temperature changes at the microscale. A similar method was employed as used in Soltys and Crimaldi (2010). Rhodamine b and sulforhodamine-101 were used as the two dyes with peak emission wavelengths of 564 nm and 615 nm, respectively. However, a Nd:YAG laser was preferred over another laser type such as an ion laser because a very high illumination intensity over a short timescale is needed to glean accurate instantaneous temperature measurements. This is because the timescale of heat dissipation at the microscale is very short and the intensity of absorbed light must be high

enough in order to measure fluorescence. With calibration and use of a pulsed laser they were able to obtain temperature measurements with uncertainties of $\sim 0.5 \circ C$, which for microscale measurements is a considerable improvement over previous single dye LIF results with uncertainties of $\sim 1.5 \circ C$.

CHAPTER III

INSTRUMENTATION AND EQUIPMENT

The tilting flume in the Environmental Fluid Mechanics Laboratory at Georgia Tech was used for both a single-color PLIF experiment and a two-color PLIF experiment, as shown in Figures 3.1 and 3.2, respectively. The goal of the single-color PLIF experiment was to compare the dye concentration of a single point of interest in the PLIF results with simultaneous conductivity probe measurements of salt concentration of the same source release. The two-color PLIF experiment was performed with two dye releases to quantify and visualize the dye concentration and interaction.

3.1 Flume

The slope of the tilting flume was adjustable via a control panel that allowed two large industrial grade screws to tilt the 24.4 meter long flume up or down. The position gauge display provided an accuracy of five decimal places. The width of the flume was 1.07 meters. The bed of the flume was once smooth but had after years of experiments become very corroded, consequently forming more of a rough bed. However, for the purpose of both experiments quantifying the exact roughness was not important. Flow to the flume was delivered via a head tank providing water to a piping system, whose flow rate was controlled via a 0.15 meter diameter gate valve and an electromagnetic flow meter. The depth of the flow in the flume, as well as the velocity, was controlled via a control panel for an adjustable tail gate.

3.2 Dyes

A single fluorescent dye (rhodamine 6G) was used for the single-color PLIF experiment and two dyes (rhodamine 6G and oxazine 725 [or alternatively called oxazine

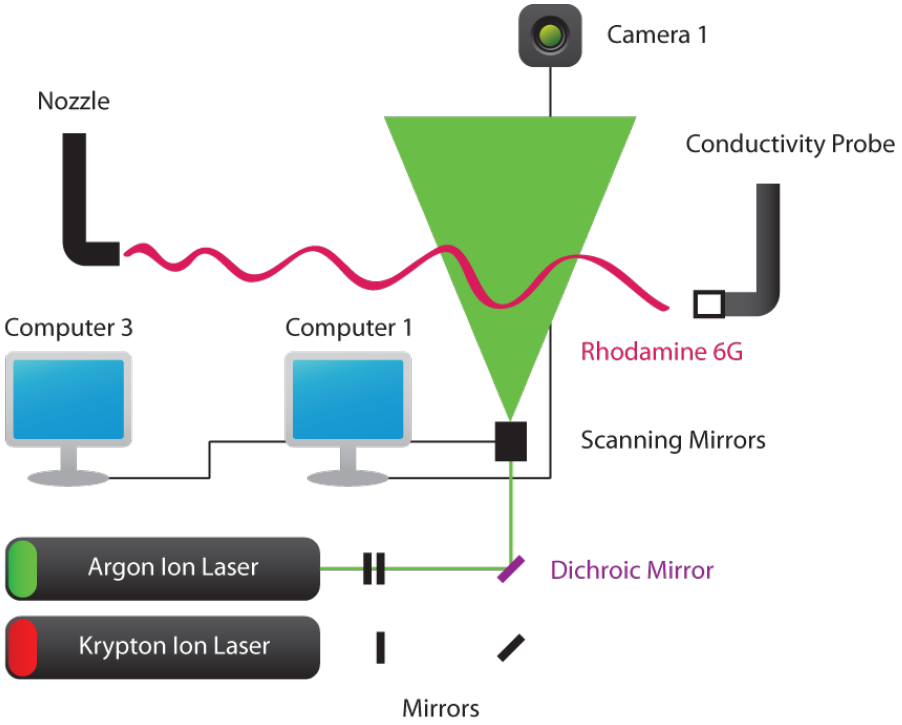

Figure 3.1: Single-color PLIF experiment setup combined with conductivity probe.

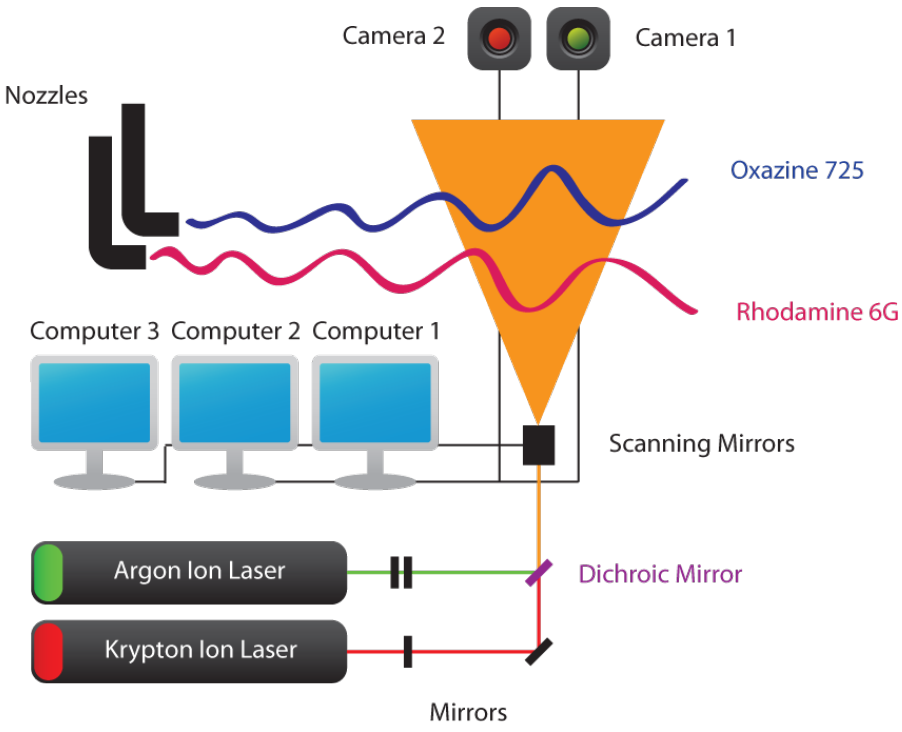

Figure 3.2: Two-color PLIF experiment setup.

1 perchlorate]) were used for the two-color PLIF experiment. The rhodamine 6G peak absorption wavelength was 530 nm and peak emission wavelength was 560 nm. Similarly, the oxazine 725 peak absorption wavelength was 643 nm and peak emission wavelength was 658 nm. Once in solution, all dyes were stored in the dark to minimize absorption of light.

3.3 Dye Delivery

For both experiments dye was released from a 0.42 cm diameter nozzle held firmly in place by an acrylic collar mount attached to a metal back plate, which was securely screwed to a heavy wooden plank resting across the top of the flume side walls. For the single-color PLIF the nozzle was located at the center of the board. For the two-color LIF, two mounting brackets were located symmetrically about the flume centerline with spanwise separation of 10 cm.

Tygon tubing connected the rhodamine 6G nozzle to a pump with a maximum flow rate of 18.5 liter per minute and a maximum head of 2.7 meters. A 30 liter open-top polyethylene container was used to hold the source mixture and was connected to the pump as shown in Figure 3.3. The height difference between pump and flume was about a meter, well within the limits of the pump. For the two-color PLIF a 57 liter bucket was hung from the ceiling in the laboratory about 3 meters above the flume, and Tygon tubing connected the bucket to the second nozzle as shown in Figure 3.4. A valve was located just below the bucket along the tubing line to allow for easy control of the source flow rate. To control the flow from each nozzle to create an iso-kinetic release in the flume flow, a metal hose clamp was attached along each tubing.

3.4 PLIF System

A planar laser-induced fluorescence system was constructed to illuminate the dye plume. It consisted of two lasers (one paired with each dye used), a series of mirrors

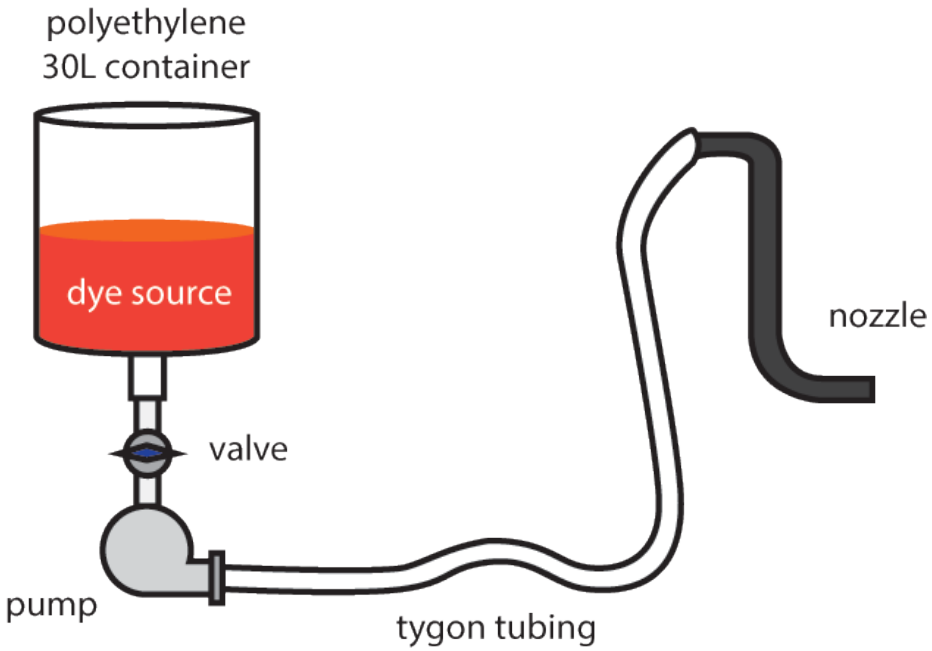

Figure 3.3: Source delivery method of rhodamine 6G dye.

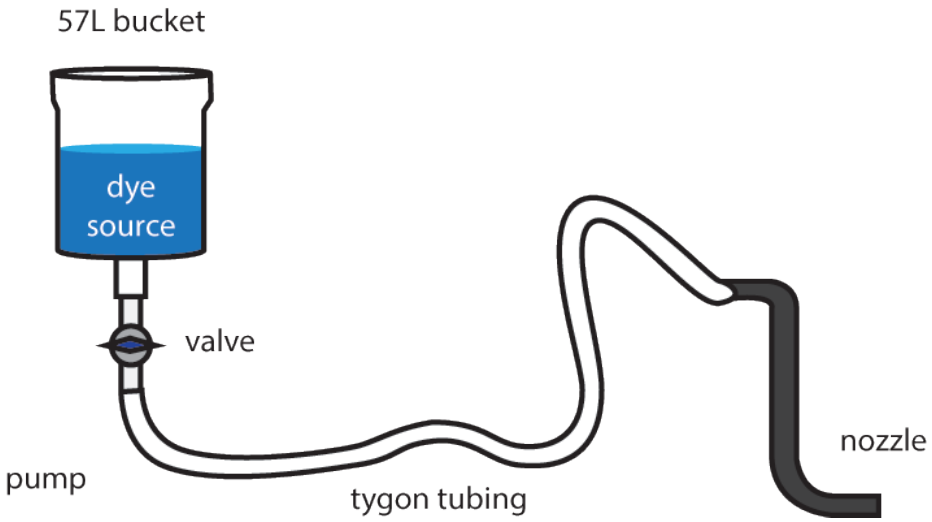

Figure 3.4: Source delivery method of oxazine 725 dye.

to align and combine the two laser beams. The second scanning mirror (y-axis) was used to set the elevation of the beams entering the flume, while the x-axis scanning mirror was used to sweep the laser beams in the horizontal direction.

3.4.1 Lasers

The two lasers used in the experiments were an older Coherent Innova Argon ion laser, which lased at 514 nm, very close to the peak absorption wavelength of 530 nm for the rhodamine 6G, and a newer Coherent Innova Sabre Krypton ion laser, which lased at 647 nm, very close to the peak absorption wavelength of 643 nm for the oxazine 725. The Argon ion laser was paired with the rhodamine 6G and the krypton ion with the oxazine 725 for this reason. Both lasers had adjustable power, shutters, and tuning capabilities. For safety reasons, each laser's power supply was connected to its own circuit breaker. Both lasers were also water cooled. Both lasers were mounted on a large metal breadboard about 1.2 meters by 1.2 meters with 48^2 $\frac{1}{4}$-20 screw holes spaced 2.5 cm apart. These screw holes facilitated mounting optical elements.

3.4.2 Mirrors and Lenses

Several mirrors were attached to adjustable stands secured at certain locations on the breadboard as shown in Figure 3.5. Two mirrors were required to adjust the height of the Argon ion laser beam to be at the same elevation as the Krypton ion laser beam. A series of mirrors were used to co-align the beams (Figure 3.5). The mirror for the Argon ion laser was dichroic, specifically allowing only the Krypton laser beam to pass through and reflecting all other light (i.e., the Argon ion beam). Once co-aligned the beams were directed to the scanning mirrors. For the single-color PLIF experiment, the arrangement was identical except only the Argon ion laser was lasing.

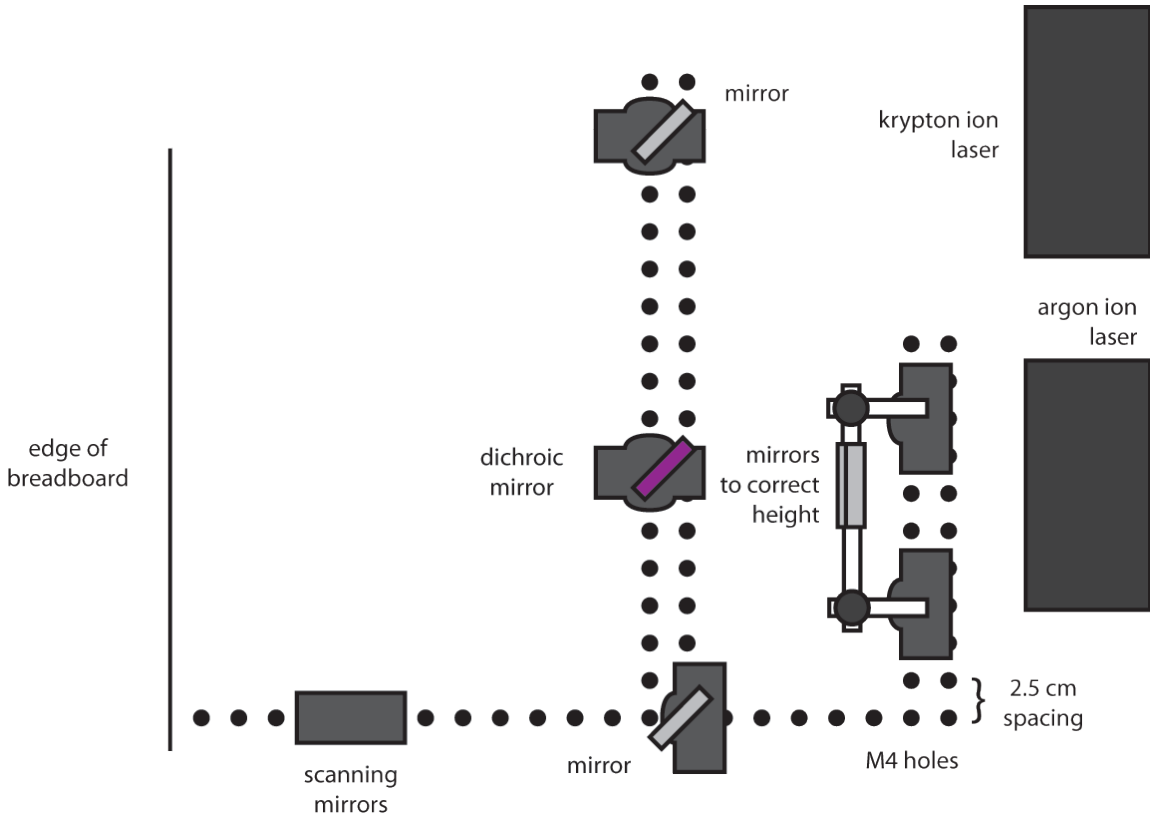

Figure 3.5: Optics setup on the breadboard for all experiments.

3.4.3 Computers

Three computers were used to perform the experiments. One was equipped with National Instruments LabVIEW software and was used to create timing signals to synchronize the data collection process. A National Instruments multipurpose module was connected to this computer via USB and controlled all voltage input and output. Additionally, one computer was used for image acquisition from each camera, respectively. These computers were equipped with two 2 TB hard drives each configured in a RAID 1 array to ensure that data was not lost or corrupted. These computers were equipped with CamWare image capturing software (Cooke Corp.) and DaVis image processing software (LaVision Inc.), which included a PLIF processing package. For the two-color PLIF the hard drive write speed, in relation to the image capture frequency, limited the bandwidth for image capture.

3.4.3.1 Software

Two custom LabVIEW VIs were created, one for each experiment. One VI synchronized a digital-to-analog output channel for the scanning mirror with one counter output channel for the image capture signal of a camera and an analog-to-digital input channel for the conductivity probe readings. The other VI synchronized the same analog output channel with two counter output channels, one for each camera. Each VI had adjustable voltage limits for the analog output channel in order to adjust the width of the x-axis scanning mirror sweep as well as adjustable frequency for the scanning mirror sweep rate and signal for image capture. The CamWare software was used to adjust the image exposure time period and set storage parameters of the captured image files.

3.4.4 Scanning Mirrors

Two scanning mirrors were mounted on an aluminum block attached to a post on the breadboard. The x-axis mirror rotated to reflect the laser beam in the horizontal

direction creating a sheet of light. A second mirror (y direction) was there to allow for three dimensional LIF by moving the reflected beam(s) up and down. This mirror, however, was fixed for all experiments. The control signal was sent from the National Instruments module to the scanning mirrors via a control and power unit and BNC cables.

3.5 Cameras

One pco.edge camera (Cooke Corp.) was used for the single-color PLIF and a second pco.edge camera was added for the two-color LIF. These sCMOS cameras captured images at a resolution of 2560 pixel width and 2160 pixel height for the single-color PLIF experiment and a total of 5.5 megapixels. However, due to the hard drive limitation, the two-color PLIF images were captured at a resolution of 1920 pixel width and 1080 pixel height in order to keep the frequency of image capture in sync by staying within the bandwidth of the hard drive write speed of around 62 MB/s. Had the bandwidth been too much for the hard drives to write by keeping the 2560 x 2160 resolution, the frequency of image capture would have been erratic and variable as each hard drive system would have been writing at its maximum. For the single-color experiment, the rhodamine 6G camera was centered and mounted to a support frame above the flume on an adjustable stage. For the two-color PLIF experiment, this camera was moved half its width to one side and the second camera was mounted next to it so that the cameras were symmetrically slightly off-center above the flume.

Different camera lenses were used for each experiment. For the single-color LIF, which required a much smaller area of interest, a Nikon AF Micro Nikkor 200 mm lens was used to create an image of approximately 3 cm by 3 cm. For the two-color PLIF a larger area was needed to properly view the interaction between the two dye plumes. As such, each camera was fitted with a Nikon AF Micro Nikkor 60mm lens.

3.6 Camera Filters

Two filters were used, one for each camera, in order to filter out unnecessary light and allow only the fluoresced light of each dye to be captured. The camera for the rhodamine 6G was fitted with a band pass filter allowing only light in the range of 540 to 570 nm wavelength to pass through. The camera for the oxazine 725 had a long pass filter to pass light above 660 nm. Each filter was attached to a custom metal ring that fit between the camera digital sensor and the lens.

3.7 Conductivity Probe

A conductivity probe was used during for the single-color PLIF experiment to collect data via a contact sensor near the PLIF area of interest. The Precision Measurement Engineering Model 125 was mounted from above and centered in the flume. The distance between nozzle and probe tip was 0.5 meters and the probe tip was just out of sight of camera view (about 1 cm). The output signal of the probe was read via the National Instruments module (A/D channel) and LabView software.

CHAPTER IV

EXPERIMENTAL PROCEDURE

The experimental procedures followed similar steps and began with setup and calibration, followed by the actual experiment. The following overview was common to both experiments. The dye calibration was performed first in order to determine what concentration of dye corresponded to near-maximum white intensity in the acquired image and consequently what the maximum source concentration for the experiments should be. Fortunately, the effects of the calibration dye in the laboratory water source were negligible due to the large volume of water in the recirculating system. The rhodamine 6G calibration procedure was repeated for the two-color PLIF since the area of interest was of a larger size, requiring a wider laser sheet which resulted in a different laser intensity per area. Because fluorophores absorb light in order to fluoresce, it was ensured that for every part of calibration and data collection that all lights were turned off to minimize any excess absorption of non-laser light by the dyes to prevent photobleaching.

4.1 Single-color PLIF comparison with conductivity probe

The area of interest was roughly 3 cm by 3 cm centered in the flume just upstream of the end of the conductivity probe sensor.

4.1.1 Setup

Before performing experiments, all surfaces were cleaned thoroughly, including the glass side walls of the flume, scanning mirrors, mirrors (including the dichroic mirror), breadboard surface, and tubing. The LabVIEW computer and the image capture computer were powered on and the custom LabVIEW VI and CamWare image capture

program were started on the respective computers.

4.1.1.1 Laser

The argon ion laser was turned on and allowed to warm up for about 5 minutes. The calibration procedure then began by randomly selecting several laser power levels and finding which one resulted in minimal attenuation in the captured images. For each new power level and each time the laser was started it was retuned in order to minimize amperage and optimize the laser for that particular power. The cooling water flow to the krypton ion laser was stopped for the duration of all calibration and data collection of this experiment and the circuit breaker for power to the krypton ion laser was also closed for safety and to ensure this second laser remained off.

4.1.2 Calibration

After testing a variety of combinations of laser power and dye concentration, a laser power of 1.0 watts was selected for use in image capture.

The region of interest in the captured PLIF images was located near the downstream edge of the image. Because the distance between this region and the tip of the conductivity probe was only 1 cm, the probe was kept out of the field of view of the camera so that filament comparison could be done during analysis. To determine the cross-stream center of the conductivity probe tip location, the camera rack was moved several centimeters downstream until the tip of the probe cover was in view of the camera and then an image was taken. By doing this an exact location was able to be found for the center as shown in Figure 4.1a.

Additionally, spatial calibration was needed. To properly correspond each pixel in any particular image to a spatial position, a grid was made and imaged as shown in Figure 4.1b. Each solid circle was 0.5 cm in diameter and spaced 1.0 cm apart. The pattern was printed on matte paper at 300 dpi in black and white using the highest quality print settings. The square grid was then cut and placed under a vertically

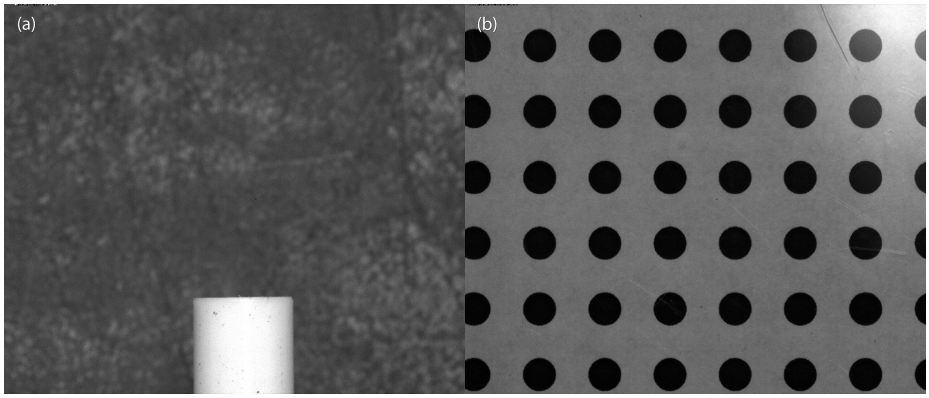

Figure 4.1: (a) Image of the conductivity probe tip used to find the horizontal center of the conductivity sensor. (b) Captured image of the grid used for spatial calibration.

adjustable acrylic sheet. The underside of the grid paper was covered with a sheet of transparency film and sealed completely with duct tape so that water would not seep in. The vertical distance from the bottom of the acrylic sheet to the bed of the flume was adjusted to the height of the conductivity probe tip.

4.1.2.1 LIF Calibration Profile

The intensity of fluoresced light is directly and linearly proportional to the dye concentration. In order to create a calibration profile for the particular relationship in this experiment, about six images for fixed concentrations were needed.

The lower concentration images were taken first to minimize error induced by residual dye. First, a 1 liter solution of rhodamine 6G and distilled water with a concentration of 0.05 mg/L was thoroughly mixed in a 2 liter polyethylene container and then poured into a 6×6×12 inch acrylic calibration container centered below the camera. The solution was allowed several minutes to come to rest and the camera was turned on along with the laser, which was then tuned to 1.0 watts. The single-color LabVIEW VI was started and the width of the laser sheet was adjusted so that each end barely passed the edges of the calibration container. Next, 100 images were saved to the computer and after capture the LabVIEW VI was stopped and the laser was turned off. The calibration solution was disposed and the container was thoroughly

rinsed with distilled water to remove any residual dye. The same procedure was then repeated in increments of 0.05 mg/L until a maximum of 0.4 mg/L was reached.

4.1.2.2 Conductivity Probe Calibration Profile

A calibration profile was created for the conductivity probe in a very similar manner to the PLIF dye calibration. Several different concentrations of salt were thoroughly dissolved in 1.0 L of deionized water by shaking the 2.0 L plastic container rigorously for about 15 minutes for each concentration. Beginning with the lowest concentration, the conductivity probe was turned on and carefully placed in the solution several centimeters above the bottom. The LabVIEW VI was run for about 10 seconds as the probe collected voltage measurements and recorded them to a file. After each measurement the probe was rinsed in deionized water and allowed to dry before proceeding to the next measurement. This process was repeated several times until enough concentration levels had been recorded.

4.1.3 Data Collection

After the calibration images were obtained the actual experiment could be performed. This process consisted of mixing the dye/salt solution to be used as the plume source, adjusting the flume flow, starting up the argon ion laser and adjusting it to emit a stable beam, starting the nozzle release of dye/salt solution, and finally synchronously capturing images and reading conductivity probe readings by running a LabVIEW VI.

4.1.3.1 Dye Source

According to the calibration images, approximately 0.5 mg/L of rhodamine 6G concentration resulted in near maximum intensity without overexposing. The source was selected to be ten times this value, so 15 liters of solution was mixed at a concentration of 5 mg of rhodamine 6G per one liter of distilled water. After the dye had

been homogenized, table salt was added to the 15 liters of solution at a concentration of 46.1 g/L. This value was recommended by Konstantin Volyanskyy as the concentration which resulted in maximum voltage reading by the probe. However, since salt made the solution more dense, isopropyl alcohol was added to get the solution roughly equivalent in density to the flume water density of 0.992 g/cm^3. By slowly adding the alcohol, it was finally determined that 4.75 L were needed to bring the salt solution of 1.015 g/cm^3 density down to the required 0.992 g/cm^3.

4.1.3.2 Channel Flow

Flow was started to the tilting flume and after allowing about 15 minutes for it to stabilize the tail gate was set such that water flowed at a depth of 20 cm. The flow rate was adjusted such that the mean velocity of the flow was roughly 5 cm/s; this resulted in a flow rate of about 0.0102-0.0110 m^3/s. The mean velocity matched the flow used by Webster et al. (2003).

4.1.3.3 Effluent Flow

The valve was opened and the pump was turned on for the dye/salt solution. The hose clamp on the tubing was adjusted until the plume became an iso-kinetic release and about a minute was given for the flow to stabilize. The resulting effluent release was roughly equivalent to that of Dickman (2008) and the plume structure was very similar with scattered filaments of dye moving downstream at the same velocity of the ambient flow of 5 cm/s.

4.1.3.4 Data Collection Parameters

After the flow was established and dye source release stabilized, a frequency of 10 Hz was set in CamWare and an exposure of 83.33 ms was set. All LabVIEW VI settings remained the same as for calibration and the VI was run until a total of 500 images were captured (50 seconds of flow data).

4.2 Two-color LIF

The two-color PLIF procedure added a second source of dye, a second camera, and a second laser. In addition, the conductivity probe was not needed. Because 60 mm lenses were used in place of the 200 mm lens of the first experiment, a different sized laser sheet was needed to encompass the full field of view of both cameras. Because of this, new calibration profiles were collected for both dyes using a much larger acrylic calibration container whose dimensions were roughly 1 meter long, a half of a meter wide, and a quarter of a meter deep. The two laser beams were co-aligned and the two cameras were aligned as well before dye concentration calibration was performed using this larger container. When these procedures were completed the two-color experiment could begin.

To co-align the two laser beams two black pieces of aluminum were held in place on two breadboard stands about 20 cm apart and 20 cm from the scanning mirrors. Each piece of metal had a 1 mm diameter pinhole in its center to allow the laser beams to pass through. All mirrors were adjusted in both horizontal and vertical until both beams made it through both pinholes at their maximum intensity. Afterwards, both stands and pieces of aluminum were removed and it was ensured that both laser beams actually were aligned.

4.2.1 Two-camera Calibration

Although the two cameras were located next to one another they had to be adjusted via their stage mounts until their view fields were almost exactly the same. Several objects were placed on the flume floor for reference to ease this painstaking process. This camera calibration procedure placed emphasis on the importance of the spatial calibration/correction which was not of great significance for the single-color PLIF images. Afterwards, the grid used for spatial calibration in the previous experiment were reimaged since a new field of view was different.

4.2.2 Two-color PLIF Dye/Intensity Calibration

A similar procedure to the single-color PLIF calibration procedure was followed to generate calibration profiles for the two-color LIF. Rhodamine 6G was first calibrated, followed by oxazine 725 after having very thoroughly cleaned the calibration container and rinsing it with distilled water several times. The amplitude of the scanning mirror sweep was again adjusted until it barely passed each end of the container before beginning the calibration procedure. For each of the two dye calibrations the other camera was turned off for the entire duration of each procedure.

4.3 Two-color PLIF Dye Sources

For simplicity, the source concentration of rhodamine 6G was kept the same at 5 mg/L. Through a series of tests, it was determined that 2 mg/L was the optimal source concentration for the oxazine 725. 15 liters of solution were used for each dye source.

4.4 Two-color PLIF Data Collection

The source solutions were created using only rhodamine 6G and distilled water and oxazine 725 and distilled water, respectively. Next, both valves to each dye source were opened after flow became steady at the same rate and velocity of the single-color PLIF experiment. Both dye releases were adjusted via hose clamp until each was an iso-kinetic release. The two-color LabVIEW VI was run and 3000 images were captured for each camera, resulting in a time series of 5 minutes of data.

4.5 Data Processing via DaVis

The majority of PLIF results utilized the LaVision DaVis software to calibrate, correct, and convert the acquired experimental images.

4.5.1 Spatial Calibration

All raw image files, including the dye calibration images and the experiment images, were loaded into a corresponding DaVis project using the LIF package. The conversion of white intensity to concentration required several steps before accurate measurements could be made. After all images had been loaded, spatial calibration was performed by utilizing the unique DaVis procedure provided by the package. The grid images captured and shown in Figures 4.1b and 4.2 were used in the corresponding projects and DaVis automatically applied the calculated spatial calibration profiles to every image in the project. By utilizing a calibration image of solid circles separated by known distances, any distortion present in the camera view, no matter how slight or insignificant, was corrected.

4.5.2 Background Subtraction

The first step in the processing of all images was to subtract a background image. An image was captured with the lens cap on in three instances (once for the single-color PLIF with the 200 mm lens and twice for the two-color PLIF with each of the 60 mm lenses). Using the "subtract" suboperation of the processing toolbox, all images were corrected by subtracting the background image.

4.5.3 Absorption Correction

To correct for die-off of laser light as it passed through the flume water in the cross-stream direction, the absorption correction feature of the DaVis software was used. The process consisted of first determining the divergence of the laser beam by finding two lines of the laser beam in the light sheet as it passed through an arbitrary but uniform concentration field, then using the intensity of the initial beam profile (first column of pixels not affected by absorption) as a reference to determine the absorption length. The final step was to automatically calculate the absorption coefficient from these two parameters used in Equation 2.34 in order to correct all image sets in every

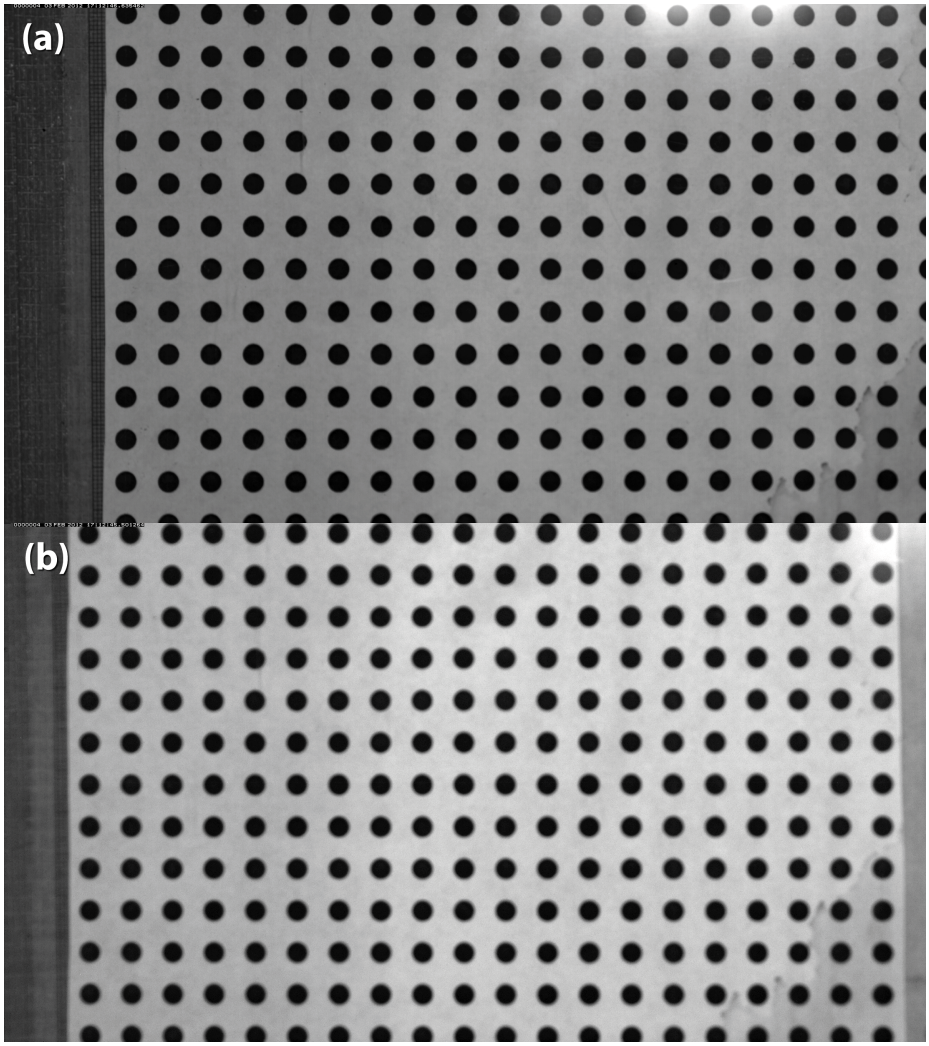

Figure 4.2: Images of calibration grid captured during the 2-color PLIF project. (a) Camera 1, used for rhodamine 6G and (b) Camera 2, used for oxazine 725.

set of data collected.

4.5.4 Dye Calibration

To directly correspond the intensity present in each image to concentration values, the concentration calibration feature of the LIF package in the DaVis software was used. First, the 100 images captured for each fixed concentration were averaged together using the average function under the statistics category of the operations in the processing toolbox. There were then eight pairs of intensity/concentration points for the single-color PLIF calibration, five different points for the rhodamine 6G calibration of the two-color LIF, and six different points for the oxazine 725 calibration. DaVis was able to calculate a linear function representing the relationship between intensity and concentration by utilizing all pairs of intensity/concentrations points from each uniform concentration field image. The generated calibration profiles are then shown in Figures 4.3, 4.4, and 4.5. Each profile had the corresponding concentration values normalized over the source concentration and multiplied by a factor of 100 to express the results in percentages to be in line with the normalized concentrations of the results. Table 4.1 shows the values and the variation of intensity present in each calibration image. The intensity counts range from 0 to 65,536 with 0 representing completely black and 65,536 representing completely white.

4.5.5 Intensity Conversion to Concentration

Once the dye concentration profiles had been generated, background image subtracted, and absorption corrected for, each image captured during the experiment could have its intensity directly converted to normalized concentration (expressed in percentage). The concentration suboperation of the LIF package used the corresponding generated linear relationships to convert every pixel intensity value in each image to a concentration percentage. All images were then exported to .dat files consisting of x-y coordinate information and a corresponding C/C_0 percentage for every pair of

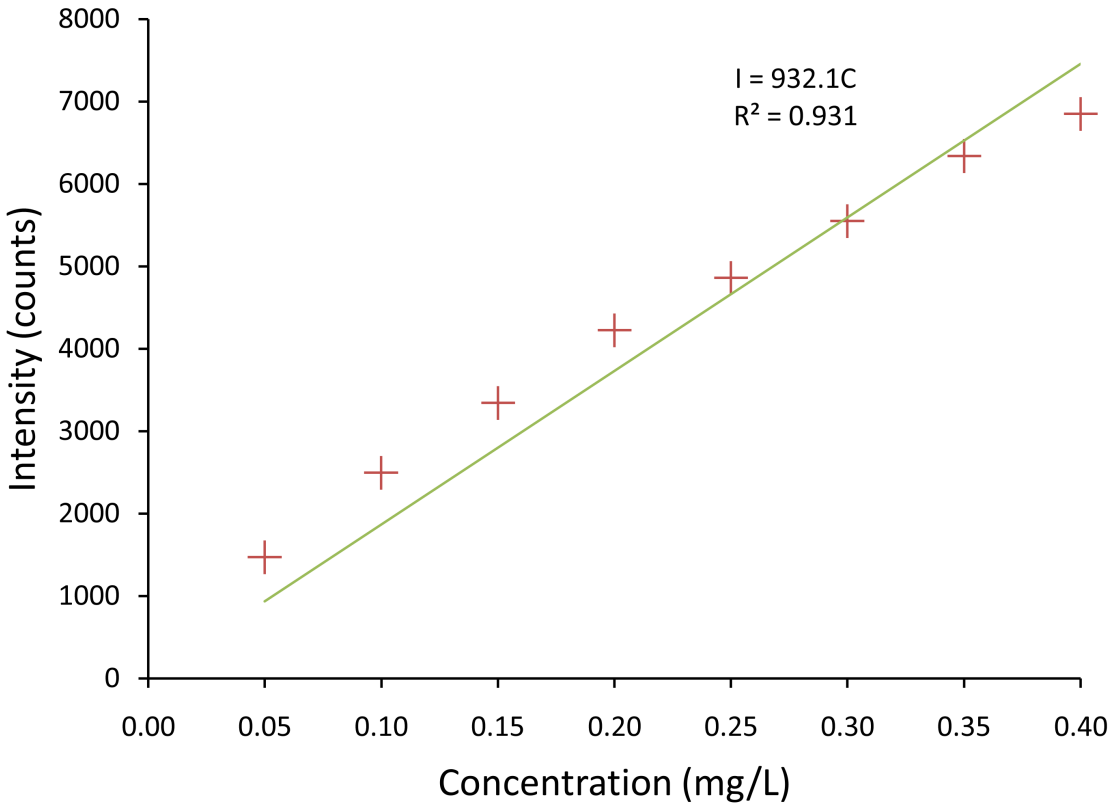

Figure 4.3: DaVis rhodamine 6G concentration calibration curve result for 1-color LIF. Red marks indicate the averaged intensity of each corrected image and their corresponding dye concentrations. DaVis fit a linear function to the points and the line is shown in green. Concentration is normalized over the rhodamine 6G source concentration and expressed in percent.

Table 4.1: Calibration concentrations expressed in percentage of source solution concentration and their corresponding averaged intensity of the resulting images for rhodamine 6G in 1-color LIF.

C/C_0 (%)	Intensity (counts)
1.00	1473
2.00	2495
3.00	3343
4.00	4225
5.00	4862
6.00	5549
7.00	6335
8.00	6852

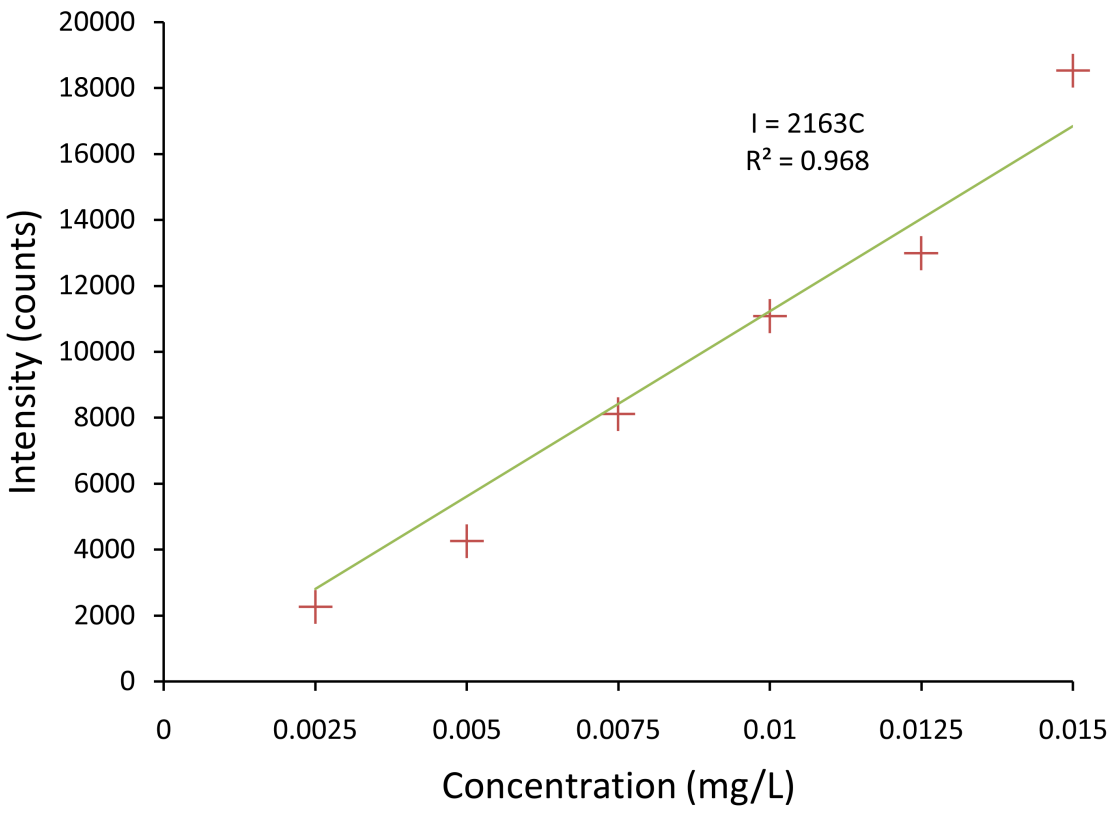

Figure 4.4: DaVis rhodamine 6G concentration calibration curve result for 2-color LIF. Red marks indicate the averaged intensity of each corrected image and their corresponding dye concentrations. DaVis fit a linear function to the points and the line is shown in green. Concentration is normalized over the rhodamine 6G source concentration and expressed in percent.

Table 4.2: Calibration concentrations expressed in percentage of source solution concentration and their corresponding averaged intensity of the resulting images for rhodamine 6G in 2-color LIF.

C/C_0 (%)	Intensity (counts)
1.67	4259
3.33	8110
5.00	11073
6.67	12985
8.33	18530

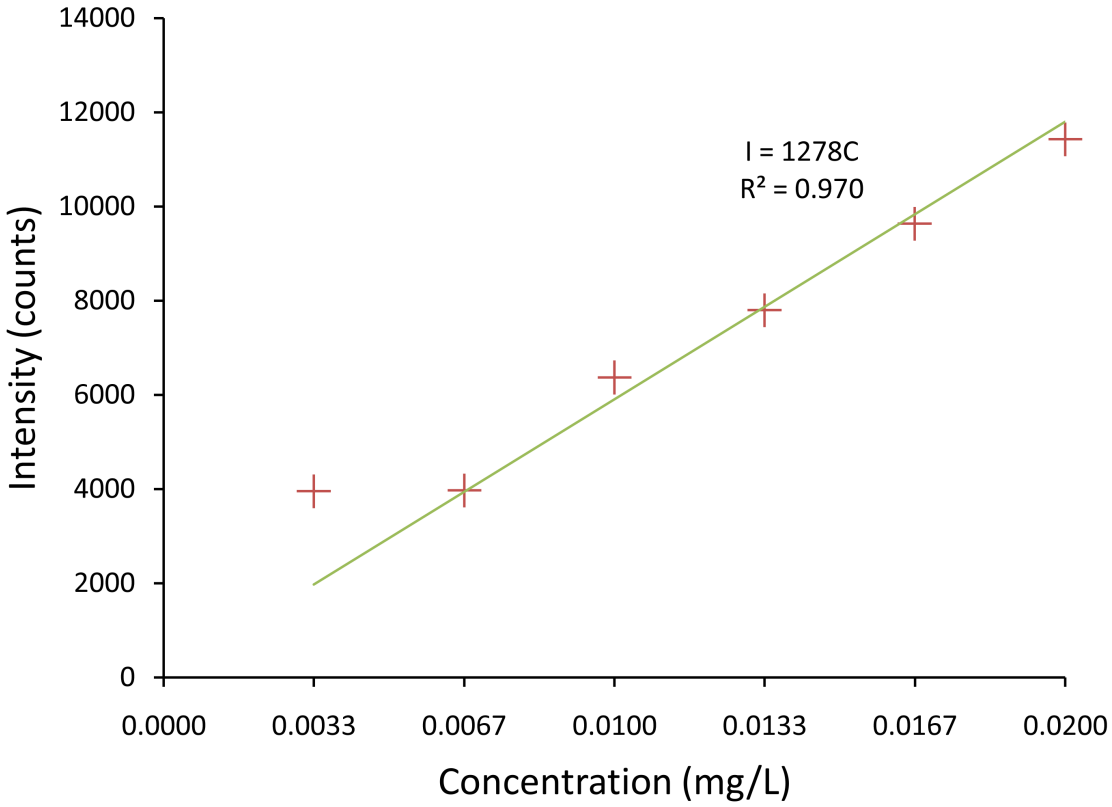

Figure 4.5: DaVis oxazine 725 concentration calibration curve result for 2-color LIF. Red marks indicate the averaged intensity of each corrected image and their corresponding dye concentrations. DaVis fit a linear function to the points and the line is shown in green. Concentration is normalized over the rhodamine 6G source concentration and expressed in percent.

Table 4.3: Calibration concentrations expressed in percentage of source solution concentration and their corresponding averaged intensity of the resulting images for oxazine 725 in 2-color LIF.

C/C_0 (%)	Intensity (counts)
2.50	3957
3.75	3970
5.00	6364
6.25	7798
7.50	9636
8.75	11428

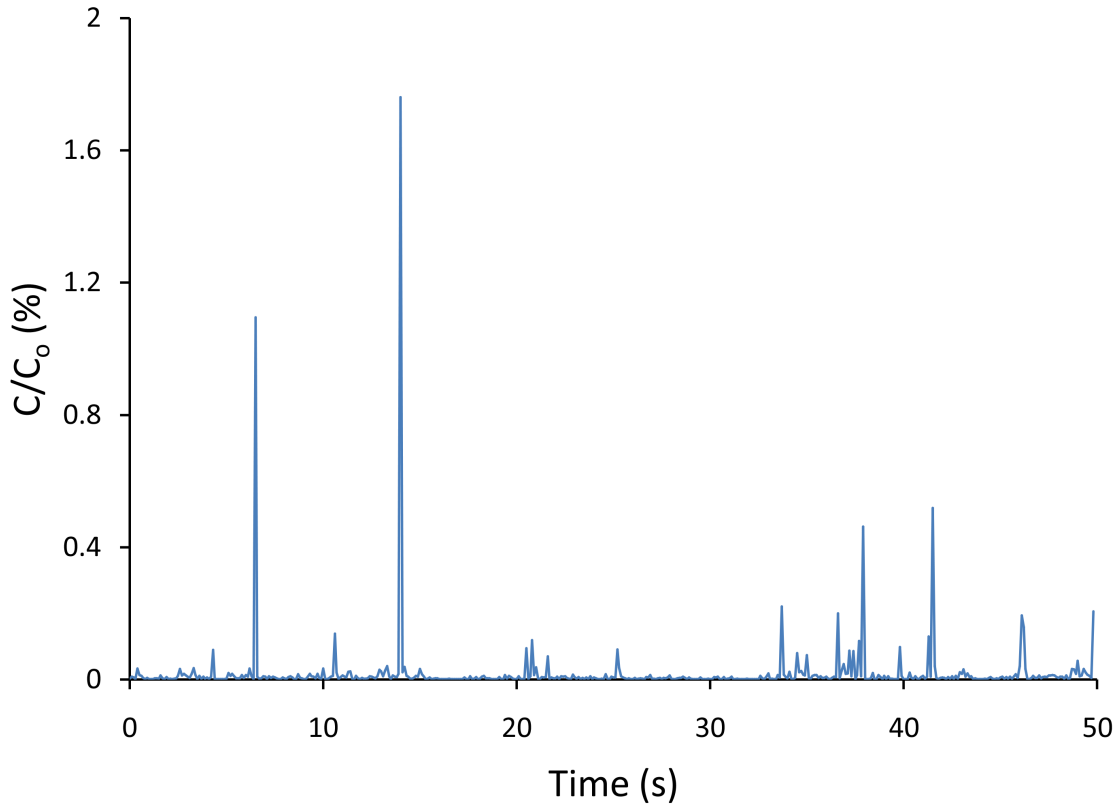

Figure 4.6: Time series of the PLIF measurements averaged over a 0.05 mm^2 rectangular area just upstream of the conductivity probe tip.

coordinates in each image of every project.

4.6 Additional Single-color LIF Operations

A MATLAB code was written to average the concentration values contained in a 1.0 mm (transverse) by 0.05 mm (streamwise) rectangle at the downstream edge of each image. This particular width was chosen to be equivalent to the width of the conductivity probe sensor. A small height equivalent to several pixels was selected to result in a more accurate value. The code used is shown in the Appendix in Figure A.1. An example time series of the concentration value averaged over the sampling region is shown in Figure 4.6.

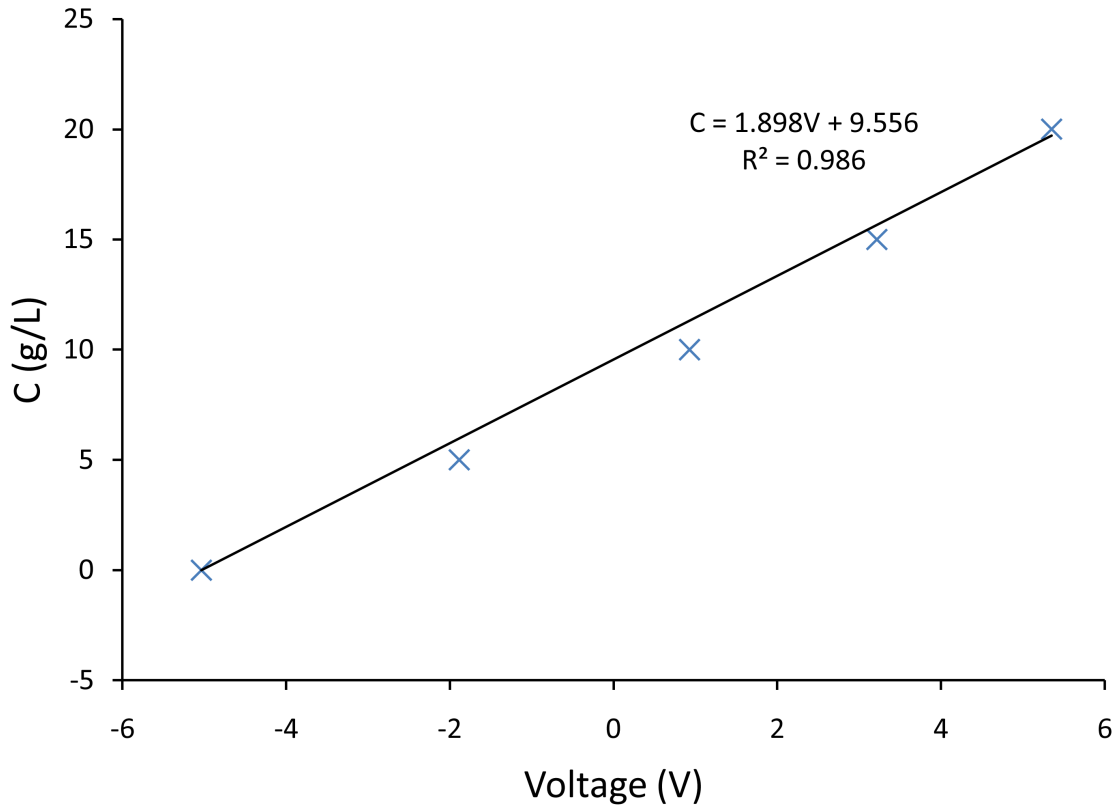

Figure 4.7: Calibration curve used to convert the experimental voltage readings to salt concentration values.

4.7 Conductivity Probe Data Analysis

The voltage readings in each of the .txt files saved in the conductivity probe calibration procedure were averaged together to produce a single voltage value to correspond to each of the salt concentrations. A simple scatter plot was created from this data and a linear fit was made with a very good R^2 value, indicating that the relationship between salt concentration and voltage was almost certainly linear. The resulting scatter plot and equation is shown below in Figure 4.7.

4.8 Additional Two-color LIF Operations

Due to the large amount of data, the .dat files were imported, manipulated, and exported in sections of 400 files at a time. Even then, each section loading required a

massive amount of memory and hard drive space for temporary files and took many hours to accomplish.

Once each block of files was loaded, a time strand was created to combine all 400 data sets into a single data set in Tecplot. Next, a logarithmic scale was chosen to be used for the $C/C_0(\%)$ scale and the steps in color intensity were rounded off for cleaner display. Blanking was used to remove the faint background tint by hiding $C/C_0(\%)$ values less than 0.05 from display. After these steps had been performed, x (streamwise) distances were converted to distances from the nozzle tips, display settings were tweaked, and the final time strand was exported to a .avi file. This process was repeated for three more sets of .dat files for a total of 150 seconds of video.

The four .avi files were imported into Sony Vegas software and text labeling was added to complete the legend. The full video was then exported using an algorithm to create a much more compressed file.

CHAPTER V

RESULTS AND DISCUSSION

Four data sets were acquired between the execution of the single-color PLIF and two-color PLIF experiments. The single-color results consisted of 500 raw images from a single camera and around 500 voltage readings from the conductivity probe. Data was collected at 10 Hz, which corresponds to 0.1 second time steps. The two-color PLIF results were a series of 3000 raw images for each of the two cameras used. However, only the first 2.5 minutes of data were used due to the sheer amount of data captured and also because 1500 images was more than enough information for the goals of the experiment.

5.1 Single-color LIF

The 50 second time series of voltages were converted to concentrations using the equation in Figure 4.7 and a time series evolution of the probe tip measurements of salt plume concentration normalized over the source salt concentration of 46.1 g/L is shown in Figure 5.1.

5.1.1 Comparison Between PLIF Results and Probe Results

Before a comparison can be made between the PLIF time series and the conductivity probe time series, correction for the spatiotemporal difference between the two data sets must be performed. There are numerous ways to go about this, but the two best are to do a cross-correlation analysis or to use the mean velocity of the flume water of $\sim$5 cm/s and the distance between the probe tip and PLIF averaging area of $\sim$1 cm to calculate a Δt of 0.2 s to subtract from the conductivity probe time values. The latter method was chosen because the spikes in concentration were quite difficult to

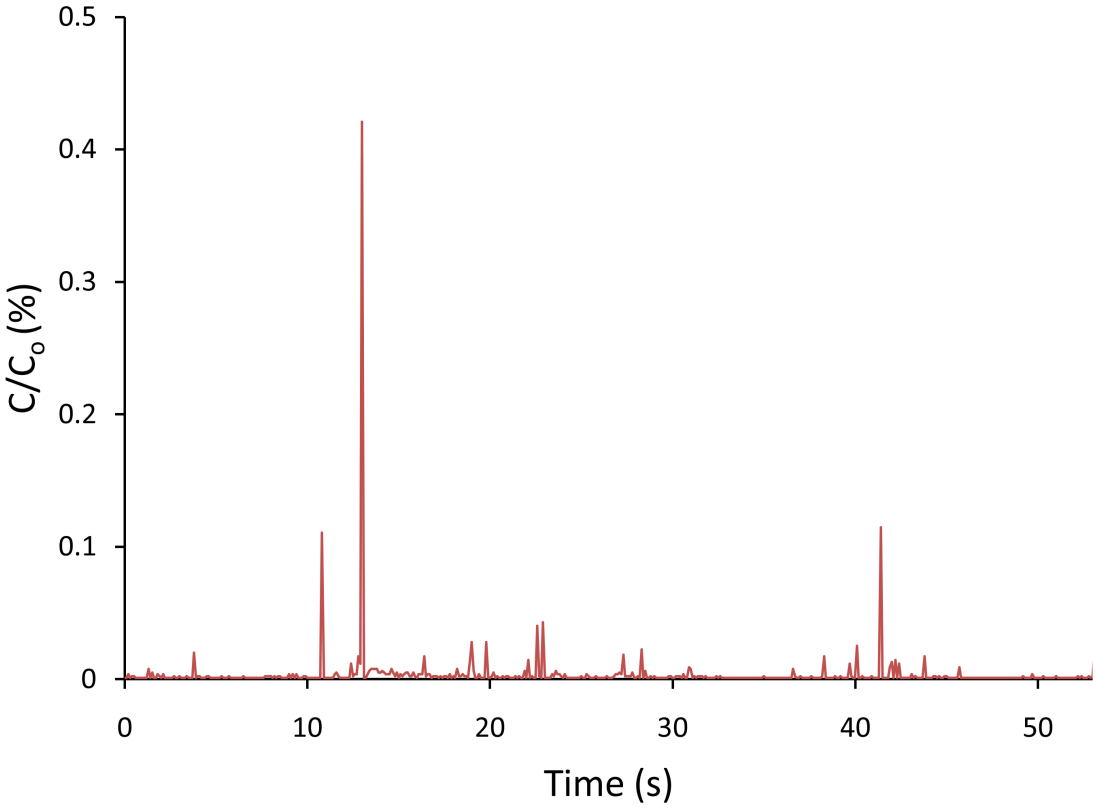

Figure 5.1: Time series of the concentration measurements collected by the conductivity probe. Concentration values are normalized by the source concentration of 46.1 g/L.

compare to one another. To further illustrate this point, Figure 5.2 plots the PLIF concentrations and the conductivity probe concentrations. Perfectly correlated data would result in a line following an equation of the form $C_{probe} = C_{PLIF}$, good correlation would result in points in the vicinity of this line, and poor correlation would result in points randomly placed across the plot. The latter is the case for our results, although there are a few points with decent correlation. Figure 5.3 shows the majority of the data with only the small spikes in concentration to give a better understanding of the correlation between the majority of the two measurement results. Due to the significant lack of correlation, using the mean velocity and distance between probe tip and averaging area was the best option to obtain the corrected time values and thus allowed both data sets to be plotted and compared. The superimposed resulted are shown in Figure 5.4.

It is interesting to note, and rather surprising, that the results are not very similar throughout the entire time series. Rather there are spikes and clusters of spikes in concentration that do appear to resemble one another, although the values of concentration are usually of different magnitude. For example, the small spikes at 10.6 seconds and 41.3 seconds are almost exactly the same value for both data sets (around 0.15% and 0.14% respectively) and the cluster of spikes from 39.9 to 43.6 seconds agree fairly well. The rest of the conductivity probe spikes mostly correspond to some sort of spike in the PLIF measurements with the exception of a few instances, most notably at 12.8 seconds where there is a large spike in the probe concentration of 0.44% whereas the PLIF measurement gives a much smaller value of 0.041%.

5.1.1.1 Discrepancy Between PLIF Results and Probe Results

There is an obvious difference between the two data sets that cannot be ignored. To further understand how and why this occurred, two areas of interest were considered. First, visually how much does a characteristic filament of dye solution change in 0.2

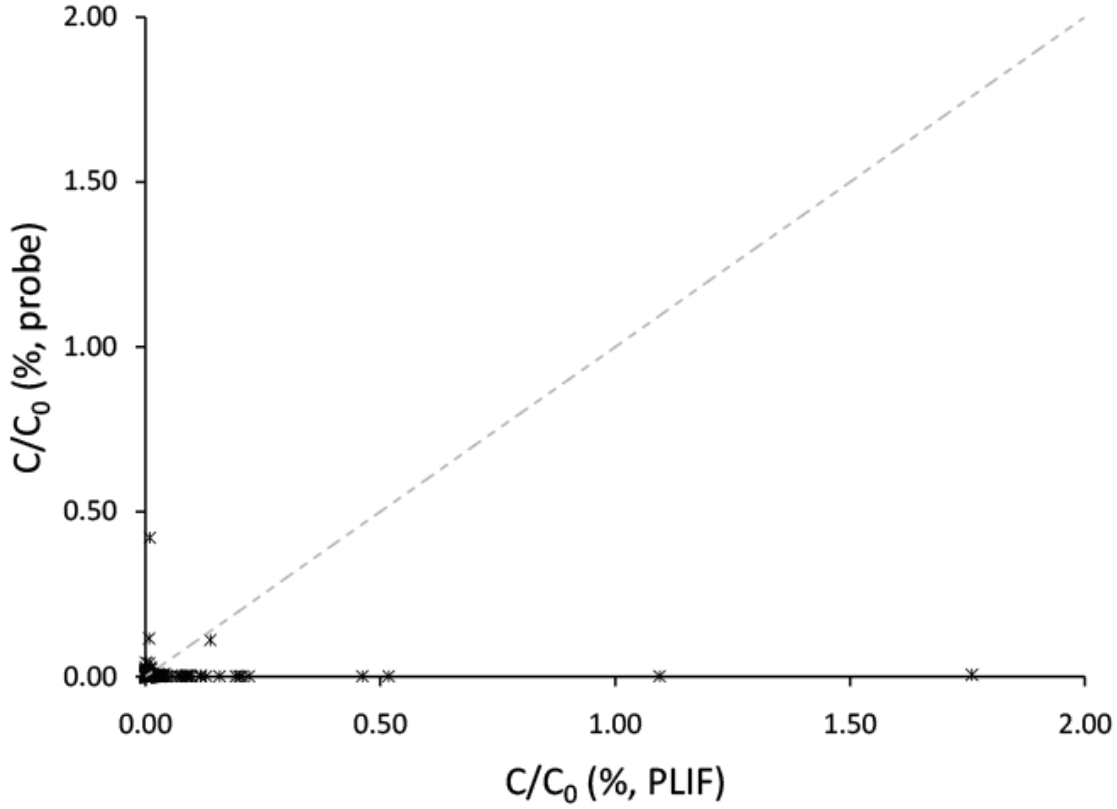

Figure 5.2: Comparison between the PLIF concentrations and conductivity probe concentrations to illustrate the major lack of correlation. The dashed line indicates perfect correlation between $C/C_0(\%, probe)$ and $C/C_0(\%, PLIF)$.

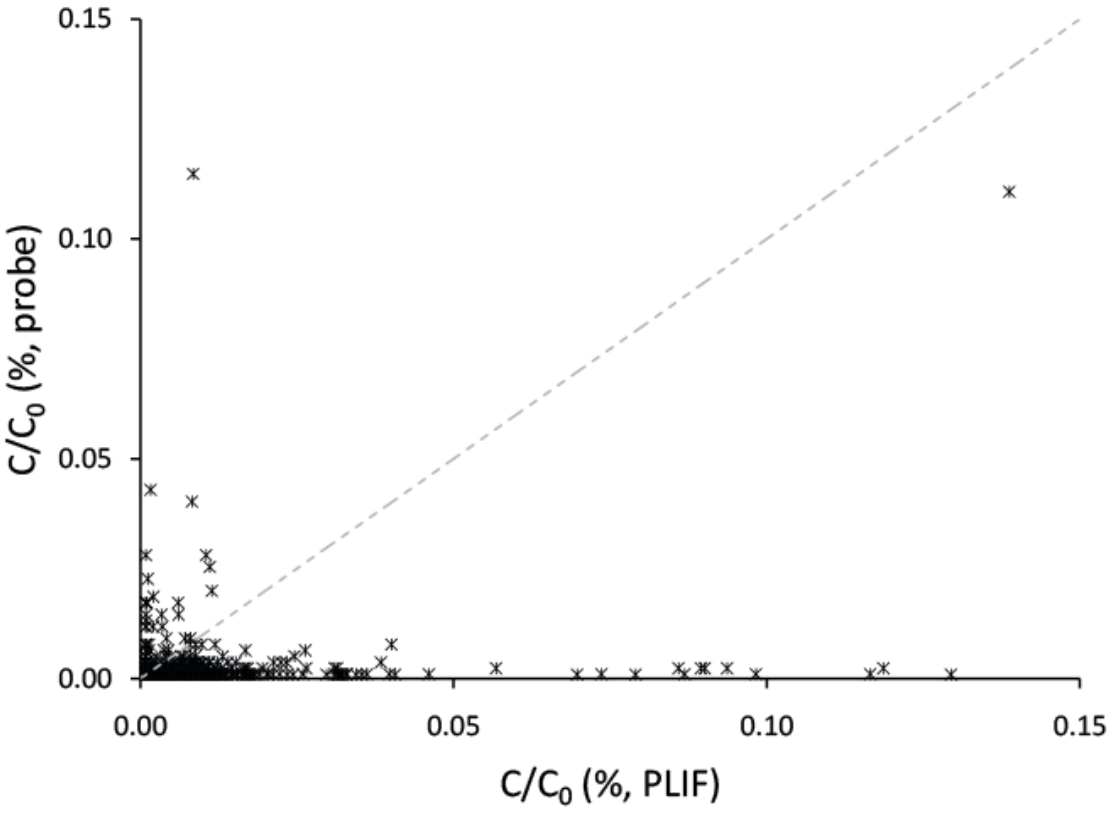

Figure 5.3: Comparison between smaller values of PLIF concentration and conductivity probe concentration to better show the correlation between the bulk of the data.

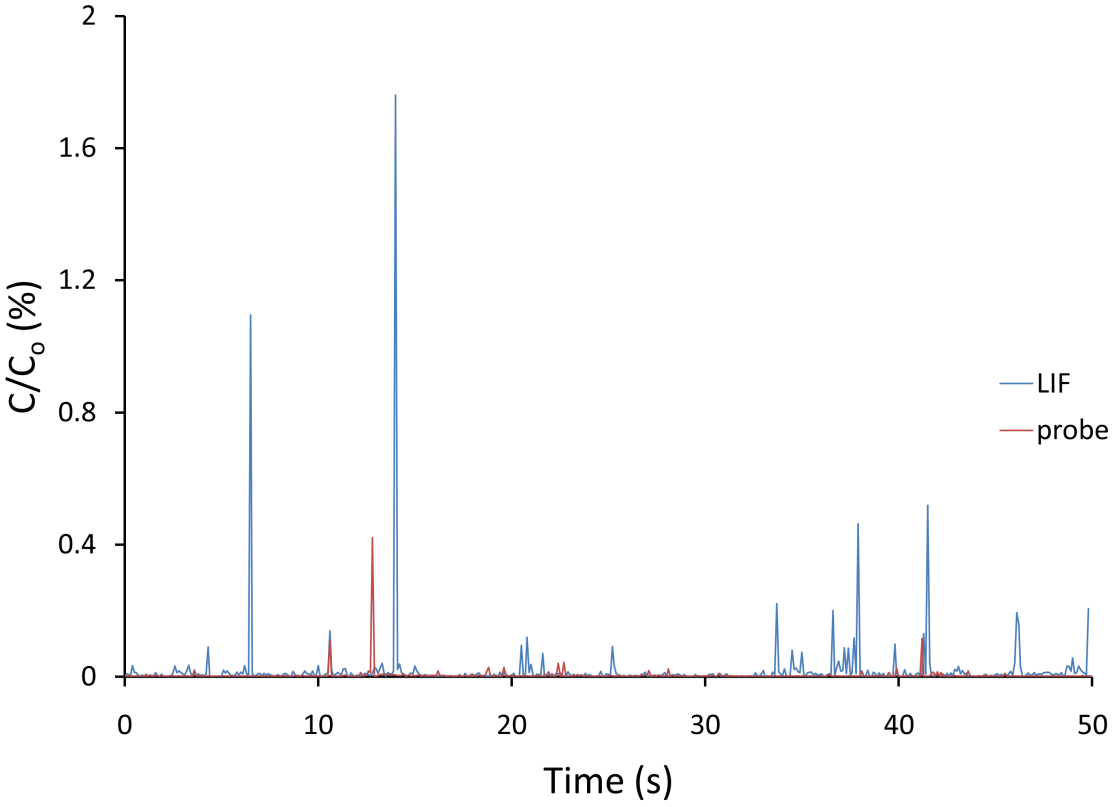

Figure 5.4: Simultaneously collected time series collected via PLIF and conductivity probe. PLIF time record is shifted to account for the advection time period between measurements locations. The normalization concentration for the PLIF data is the rhodamine 6G source concentration, whereas the normalization concentration of the conductivity probe data is of the salt source concentration.

seconds or ∼1.0 cm of movement? Secondly, how much difference is there between an averaged area of dye filament as it moves this 1.0 cm distance? By examining how much a filament changes in size, twists and turns, and moves out of plane in two frames and knowing the numerical difference between measurements of this area of the plume as it moves 1.0 cm downstream, a better understanding of why the two data sets have these discrepancies may be gleaned.

Dickman (2008) experienced a similar issue when attempting to measure odorant concentration near the outer chemosensory organs of blue crabs via 3D LIF. Shadowing effects and reflections due to the crab body made direct concentration measurements not possible. Instead, a similar method to our PLIF averaging area was employed by using much larger sampling volumes to calculate concentration centroids just upstream of the blue crab and near the mouth region. From these data and the crab location, a bias was calculated toward either side of the crab. This method was successful in determining crab response quite consistently because only the general plume and filament evolution was needed. Unfortunately, our application essentially required comparison between very accurate point measurements, and any attempt to correct for the spatial separation between averaging area and conductivity sensor to result in comparable/correlated concentrations was nearly impossible; this issue is addressed in thorough detail shortly.

In Figures 5.5 and 5.6, two filaments are examined and it is clear that some regions of the filament may change rather rapidly in a distance of only 1.0 cm whereas other regions may remain relatively unchanged in shape and/or size. There is also a slight difference in concentration judging by the red intensity. This intensity difference may be attributed to two influences. First, the dye is dispersing very slightly as time progresses. Secondly, and more of a factor, the dye filaments are moving out of plane due to turbulent stirring. Even a small vertical displacement affects the visible intensity to some degree. Figure 5.7 shows the time record for two sampling

regions separated by 1.0 cm and shifted by 0.2 seconds. The figure clearly shows how much difference a distance as small as 1.0 cm may make. The difference between the two largest spikes of dye concentration in each data set, which occurs at 14.0 seconds, has a value of 0.5%, roughly 30% the value of the largest spike. There are other occurrences where larger spikes in concentration are completely absent from the other matching points. Examples of this occur at 3.2, 33.0, and 39.8 seconds. On the other hand, other areas are almost identical, although they are far fewer in frequency. A good example occurs at 41.6 seconds with a difference in normalized dye concentration of only 0.0056% or 8.8% of the largest of these two spikes. This issue is further illustrated in Figure 5.8 where a red box is representative of the averaging area and the size of what the conductivity probe sensor would be. It is clear that due to turbulent stirring, the filament within the sampling area on the right is completely missed by the same sampling area 0.2 seconds earlier and 1 cm upstream.

However, filament change is not the only reason for the results of Figure 5.7. They may also be attributed to the slight variation in velocity of the flume water carrying the dye downstream. Because an average velocity was used for all measurements, these small differences in velocity may appear as slight variation in the characteristic peaks concentrations. Instantaneous velocity measurements were not made in order to calculate the proper distance (close to 1.0 cm but not precisely) to use for the location of the averaging area for each 0.2 second time step. For flow velocities very close to the mean velocity, concentration measurements were closer to one another.

Further discrepancies between the probe measurements and the PLIF measurements may be attributed to a few other factors as well. There seem to be quite a few drops in the conductivity probe measurements that fall below the "zero concentration" line. The probe measurements also seem to not capture as many spikes as the PLIF measurements. As such, there may have been some sort of electrical noise or a grounding issue in the probe measurements. However, the other major contributing

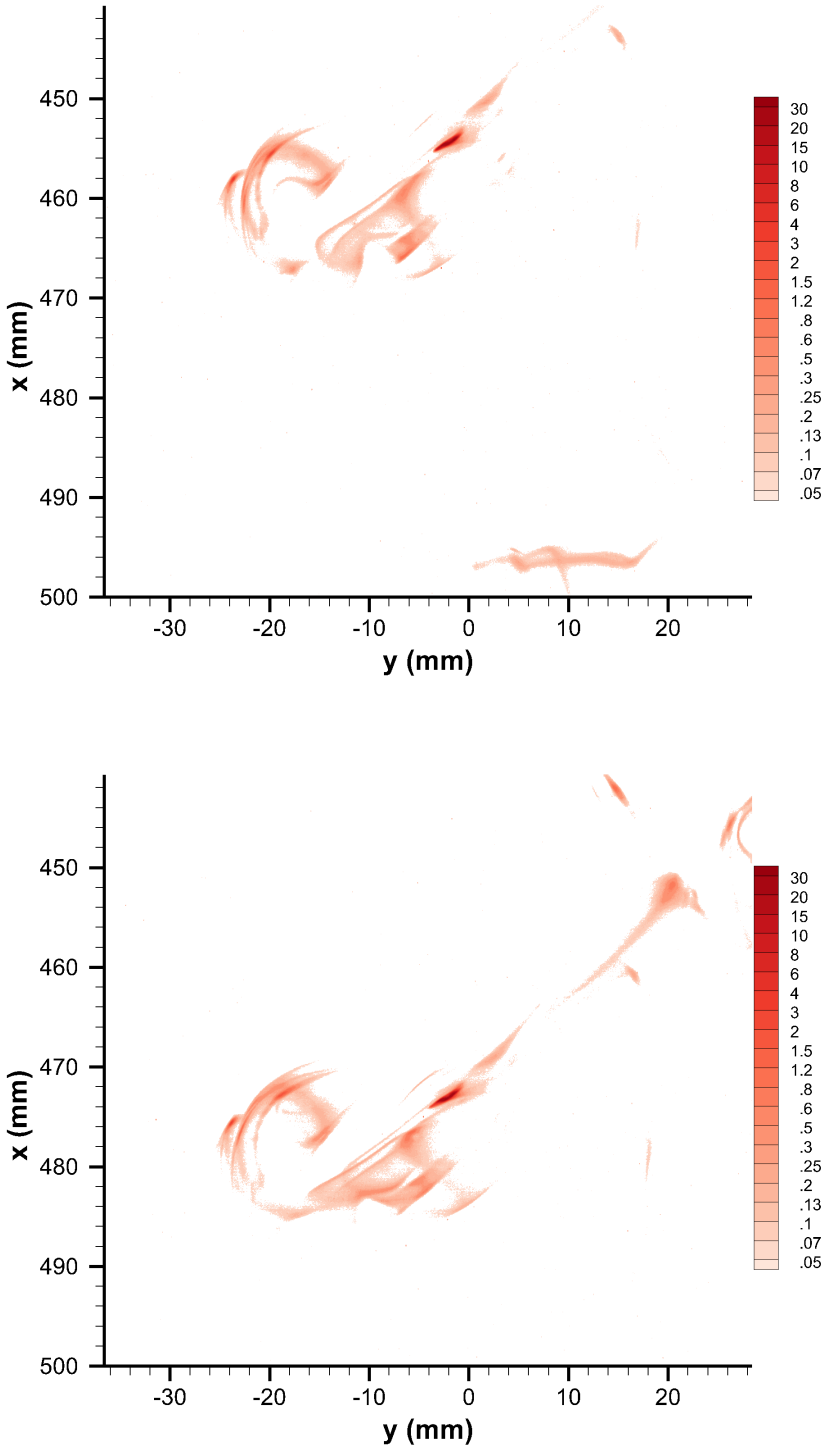

Figure 5.5: Example of concentration fields collected 0.2 s apart. The fields illustrate the evolution of the dye filament as it moves approximately 1 cm downstream (i.e., positive x direction).

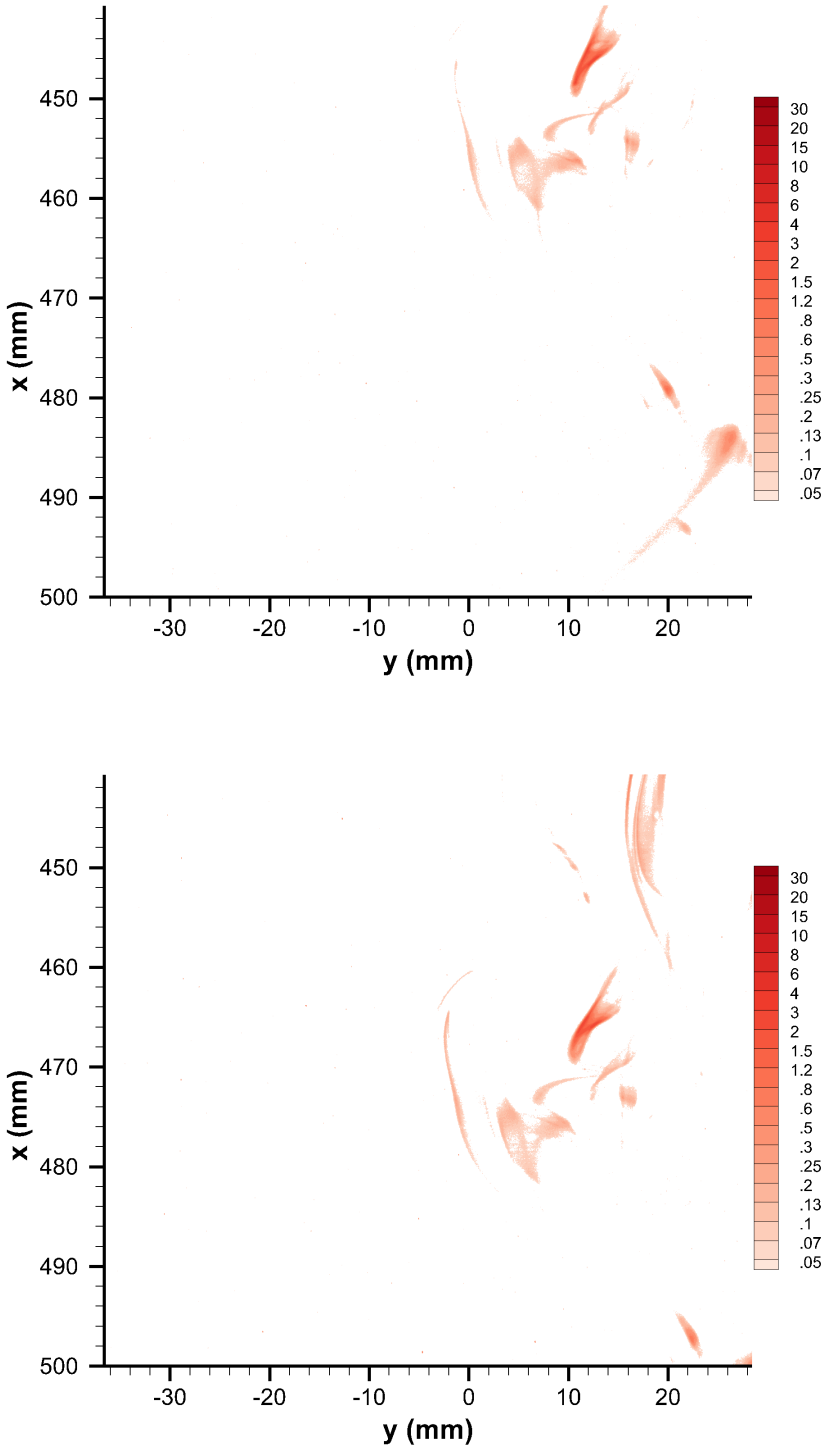

Figure 5.6: Second example of concentration fields collected 0.2 s apart. The fields illustrate the evolution of the dye filament as it moves approximately 1 cm downstream (i.e., positive x direction).

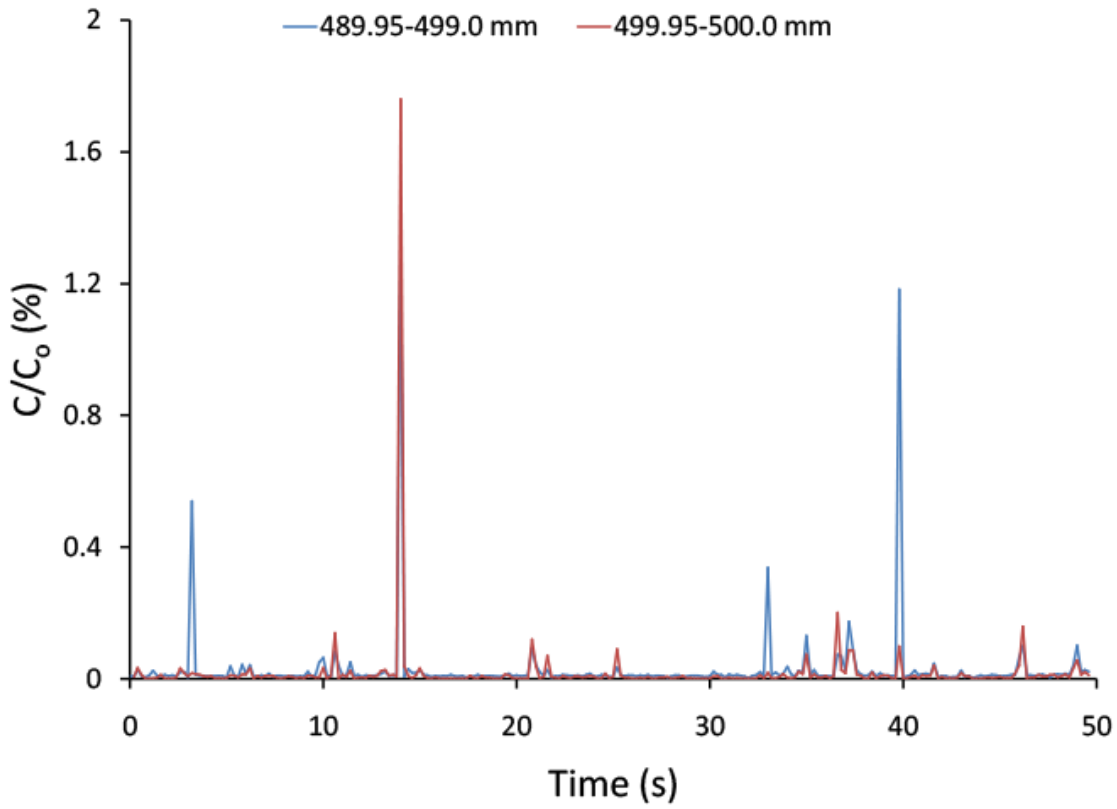

Figure 5.7: Time series for two comparable averaging areas spaced 1 cm apart in the streamwise direction. The time series of the downstream area is shifted by 0.2 s to account for the advection period.

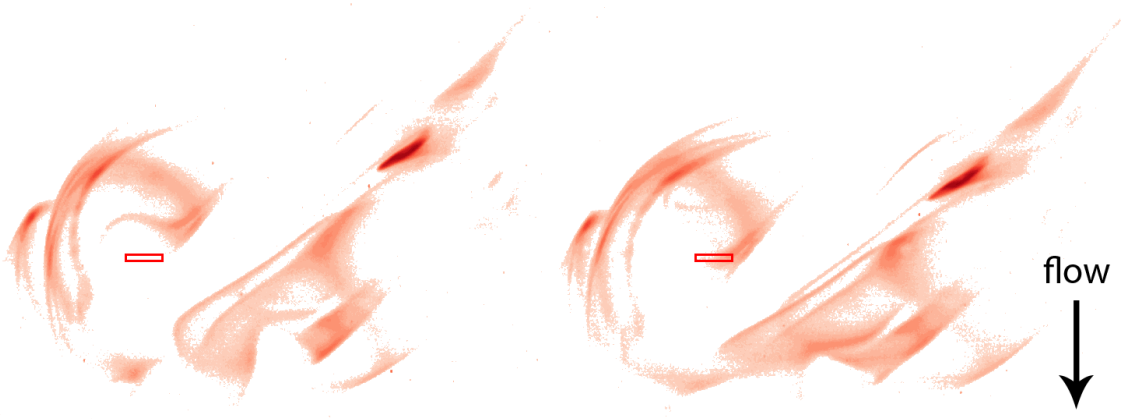

Figure 5.8: Enlarged area of Figure 5.5 illustrating how it is possible for a small filament to be completely missed by the conductivity probe located 1 cm downstream and collecting samples 0.2 seconds later than the PLIF collection.

factor to the discrepancies was due to the plastic shielding present on the end of the conductivity probe. In addition to causing a 1 cm separation distance between measurement locations, this shielding could have altered the flow around the probe tip and the accuracy of the probe measurements when comparing these measured concentrations to any other PLIF measurement upstream of the probe.

Additionally, there was a buildup of salt residue on the outside of the tubing and connectors that presented itself long after the experiment had been performed even though the salt was thoroughly dissolved in the dye solution. If the source solution was indeed lowered somewhat due to losing salt in the pump, tubing and connections between the time when the source solution was mixed and when the experiment began, then a source concentration of 43.1 g/L might have been lower in reality at the time of performing the experiment. This would result in the normalized salt concentration (C/C_0) values being smaller than they should be. As shown in the previous Figure 5.4, the probe values are indeed slightly lower than their PLIF measurement counterparts the majority of the time, with far fewer values actually being larger (which can be explained by the phenomenon illustrated in Figure 5.7).

However, the bulk of the discrepancies between the probe measurements and PLIF measurements is brought on by the evolution of filaments due to turbulent stirring over the 1 cm distance as well as the plastic shielding surrounding the conductivity probe sensor. The former is proven via differences between PLIF areas of concentration (Figure 5.7) by how seemingly random one measurement sometimes is larger than the other and at other times may be smaller. However, the separation distance seems to only account for the differences between magnitude of concentration measurements. It does not account for other differences such as the fewer high concentration measurements. If the flow was shifted around the conductivity probe shielding even slightly before reaching the sensor tip, this could possibly be the largest contributing factor for why the probe measurements do not seem to register as many spikes. However,

the length of the time series was not long enough to certainly conclude whether the lower amount of spikes in concentration was just coincidence or not.

Due to the nature of the discrepancies between the comparable values of the two data sets, it is impossible to obtain very similar values. This, unfortunately, was the purpose of this particular experiment. The only valuable information that may be gleaned is that there are similar spikes in concentration in the two measurement methods.

To obtain more comparable results the area of interest of the PLIF concentration field would need to be within millimeters of the conductivity probe tip, which would be impossible due to the plastic shielding protecting the probe sensor. The plastic shielding should have been removed to yield closer results.

However, the mean concentrations and standard deviations of the conductivity probe measurements and the PLIF measurements should be comparable along with other statistics describing time-averaged concentration measurements. Although the two points of measurements were separated by 1.0 cm, this distance is negligible in our case when comparing statistical values of the plume structure. For illustrative purposes, Figure 5.9 shows that for x/H values between 2.45 and 2.5 (consistent with our experiment), the mean concentration field remains very consistent. It is not until much further downstream (x/H values > 3) that the field begins to taper off and where differences between point measurements 1.0 cm apart would begin to show.

Unfortunately, valid statistics could not be achieved because only 50 seconds of data were recorded specifically for the instantaneous concentration comparison. Webster and Weissburg (2001) show that it takes over 5 minutes to obtain a fairly accurate mean concentration and it is not until around 10 minutes that the mean concentration converges to a very precise value. Figure 5.10 shows that 50 seconds is actually not even reasonable in estimating a proper mean concentration because different 50 second sample periods result in a very broad array of mean concentrations. If a long

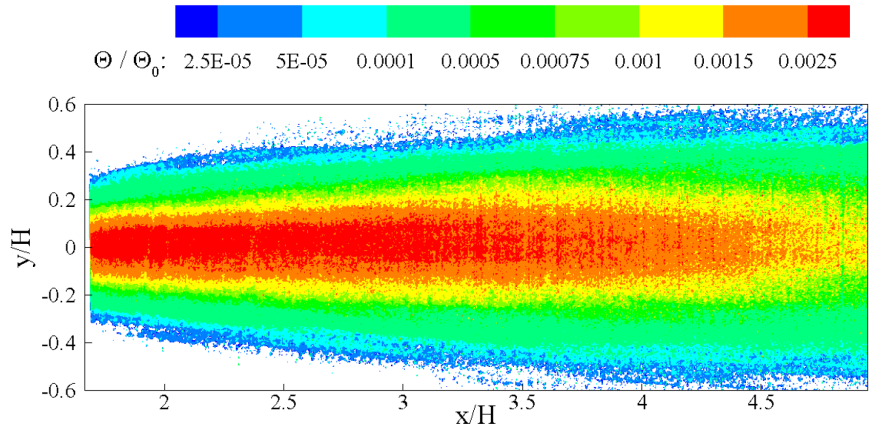

Figure 5.9: Concentration field cross-section from Dickman (2001) consistent with our flow/flume parameters taken at a distance of 2.2 cm above the flume bed.

time series of concentration data are divided into two bins and the data is indeed reasonable, the mean concentration of those two bins should be relatively close to the overall mean concentration. If this procedure is followed for the 50 seconds of data, the PLIF means of the two bins are 0.0202 and 0.0164 and the overall mean concentration is 0.0188, whereas the conductivity probe means are 0.005 and 0.003 and the overall probe mean concentration is 0.004. Two conclusions may be drawn from these results. The first is that the difference between the mean bin concentrations and the overall concentrations for both PLIF and probe data have significant differences between one another. The second is that the PLIF mean is much larger than its probe counterpart. This is consistent with Figure 5.4 whereby the PLIF data captures more spikes in concentration than the conductivity probe data, thus creating a higher mean concentration value. Both conclusions support the fact that 50 seconds of data is not long enough to obtain a valid mean concentration or any statistics for that matter.

Table 5.1 shows the full range of statistical data calculated for the two data sets. The large standard deviations for both data are indicative of large variation in concentration and support the intermittent nature of this passive scalar evolution even though they are not fully resolved and may not be accurate. It is also interesting to

Table 5.1: Calculated statistics for the PLIF concentrations and conductivity probe concentrations derived from the measurements.

-	$\bar{C}$ (PLIF)	$\bar{C}$ (probe)	σ_C (PLIF)	σ_C (probe)
Bin 1	0.020	0.005	0.131	0.029
Bin 2	0.016	0.003	0.053	0.008
Overall	0.019	0.004	0.100	0.020

note that the maximum concentration of the PLIF data is much larger than the conductivity probe maximum, although, again, most of these statistics are not accurate and only provide a rough framework for the true statistics.

This framework may best be represented by a histogram or probability density function (PDF) as shown in Figures 5.11a and 5.11b, which utilize the normalized concentrations of the PLIF and probe data divided by the standard deviations of PLIF and probe concentrations. It is clear from these figures that the concentration distributions both follow what could be described as an exponential decay, although with a longer time series of data this distribution would become more clear and the occurrences would form a much smoother and more accurate decay from which a representative function could be derived. It is also interesting to note that the PLIF and conductivity probe distributions are strikingly similar; this indicates that both measurement techniques acquired very similar intermittent behavior of the plume, which is characterized by the large density of near-zero $(C/C_0)/\sigma_C$ values quickly tapering off to near-zero random occurrences of larger $(C/C_0)/\sigma_C$ values. Rahman (2002) shows similar concentration distributions, albeit with data collected with differing roughness on flume beds. Figures 5.12a 5.12b are quite similar to our histograms except for the distribution being derived from much longer time series and having more points and thus more accurate distributions.

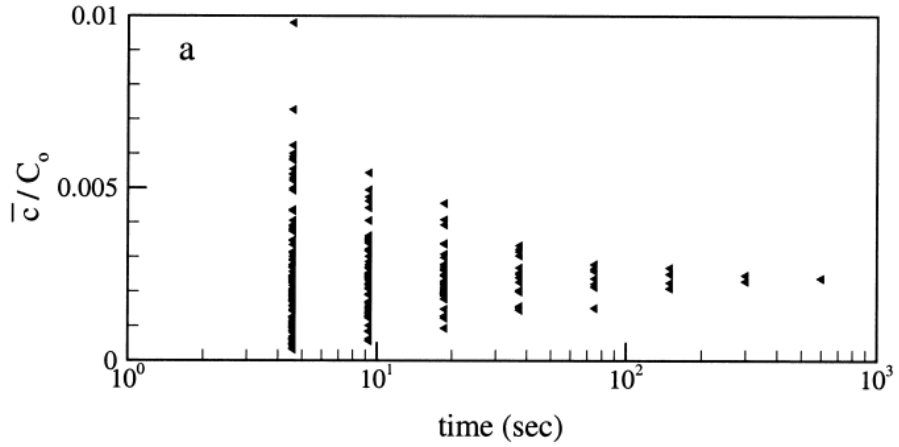

Figure 5.10: Time-averaged concentration as a function of sampling period at a point in the concentration field (Webster and Weissburg 2001)

5.2 Two-color LIF

Two-color PLIF data were collected at 10 Hz for a duration of 300 seconds. The first 150 seconds of data was manipulated and converted to concentrations in sections of 30 seconds.

5.2.1 Two-color PLIF Dye Plume Interaction

Figures 5.13, 5.14, 5.15, and 5.16 show that the plume structures remain largely on their respective sides of the channel. On occasion filaments are stirred across the centerline of the image. On these occasions, the blue and red contours sometimes overlap. It is expected that the plume interaction will increase farther downstream as the turbulent stirring process continues to expand the volume occupied by the plume structure. Increased overlap of the plume structure is also expected if the nozzles were closer together.

From Figure 5.13 faint signs of mixing may be seen near the center of the image. However, as indicated by the majority of all regions of interaction, and most particularly in Figure 5.16, the rhodamine 6G intrusion to the oxazine 725 plume structure seem to prefer to fill the voids or areas of weaker oxazine 725 concentration. This is

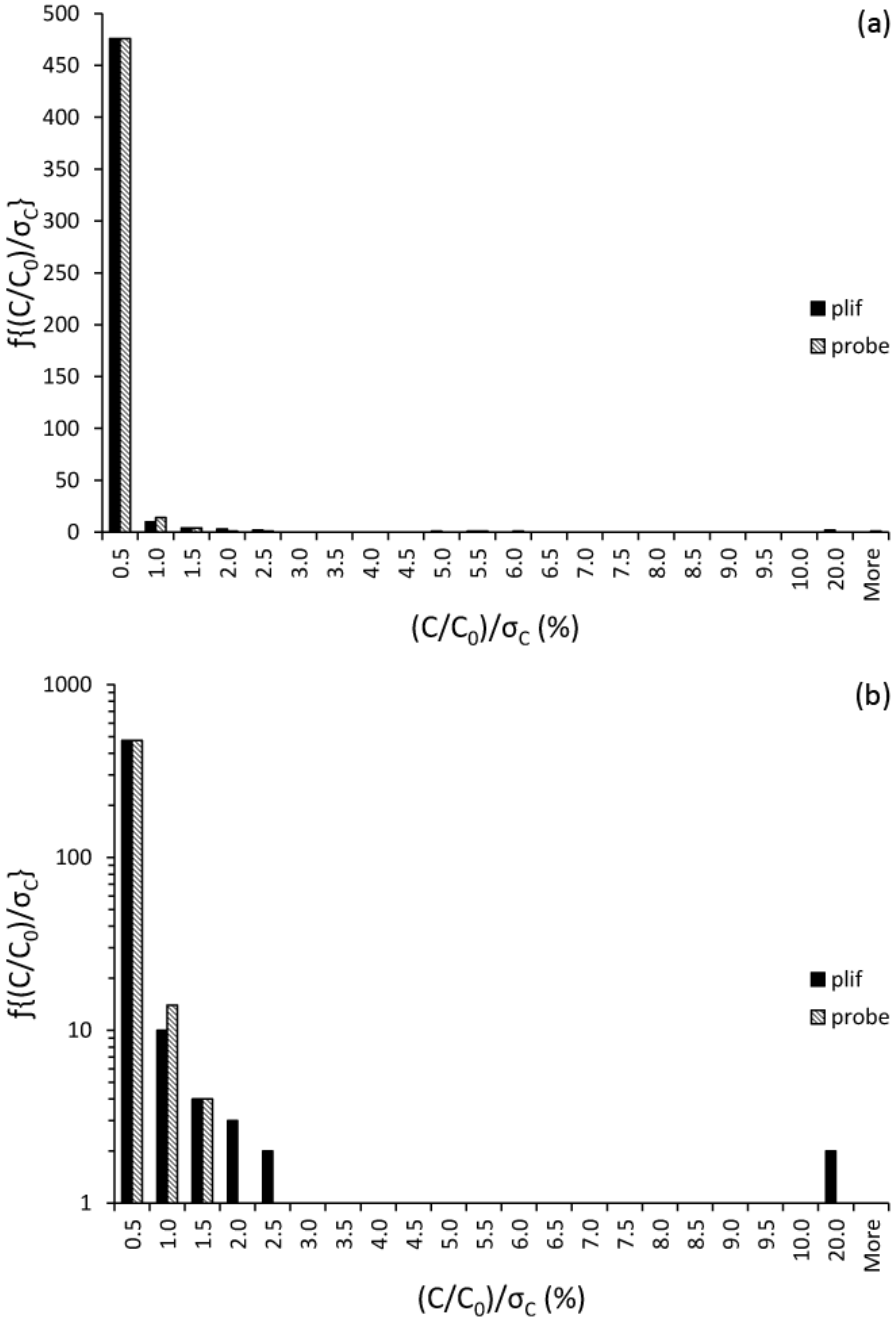

Figure 5.11: (a) Histogram derived from both PLIF and conductivity probe concentrations and the standard deviations of both data sets. (b) Same histogram with logarithmic frequency (y-axis) scale.

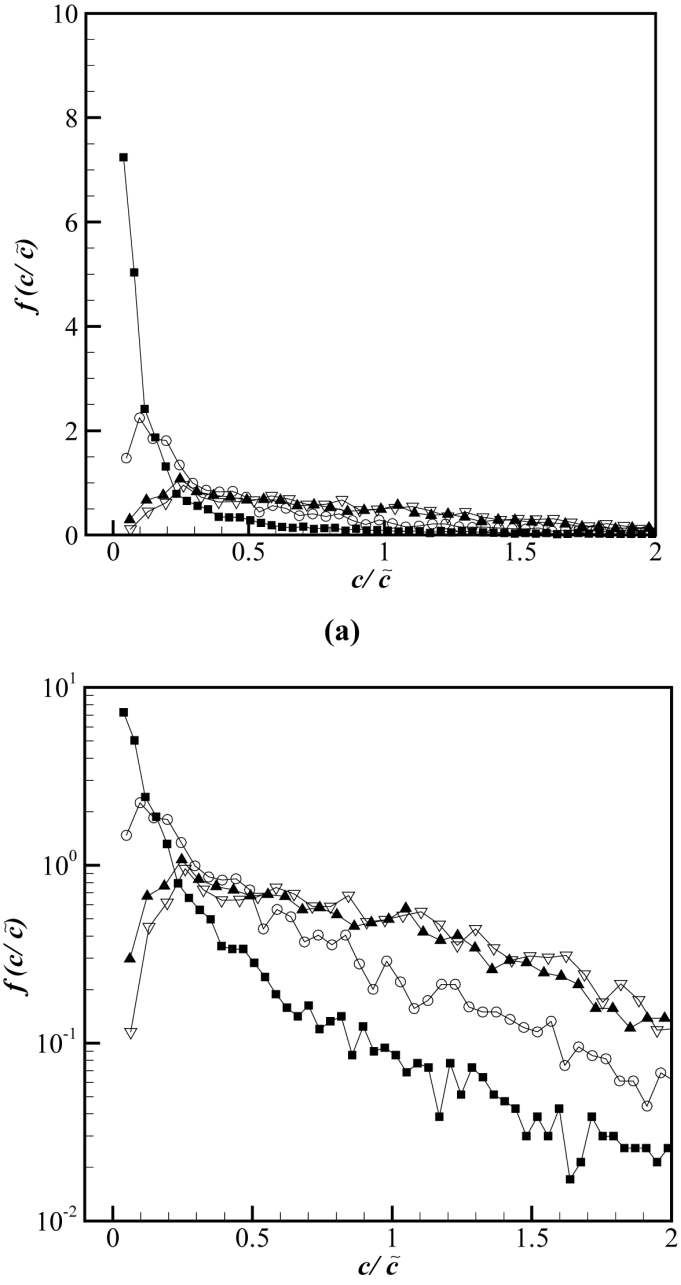

Figure 5.12: (a) Probability density function derived from LIF measurements for differing bed roughnesses. (b) Same density function with logarithmic y-axis scaling (Rahman 2002).

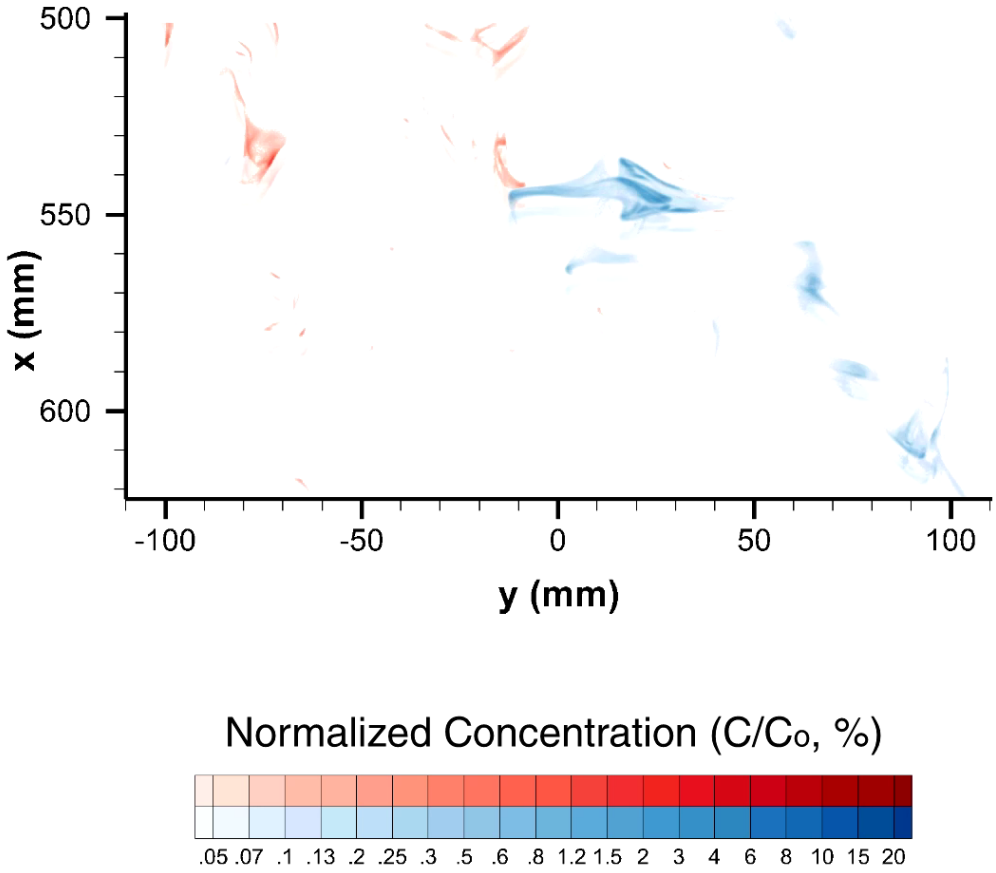

Figure 5.13: Example of simultaneously-collected concentration fields that show the interaction between the rhodamine 6G and oxazine 725 dye plumes (at 59.1 seconds).

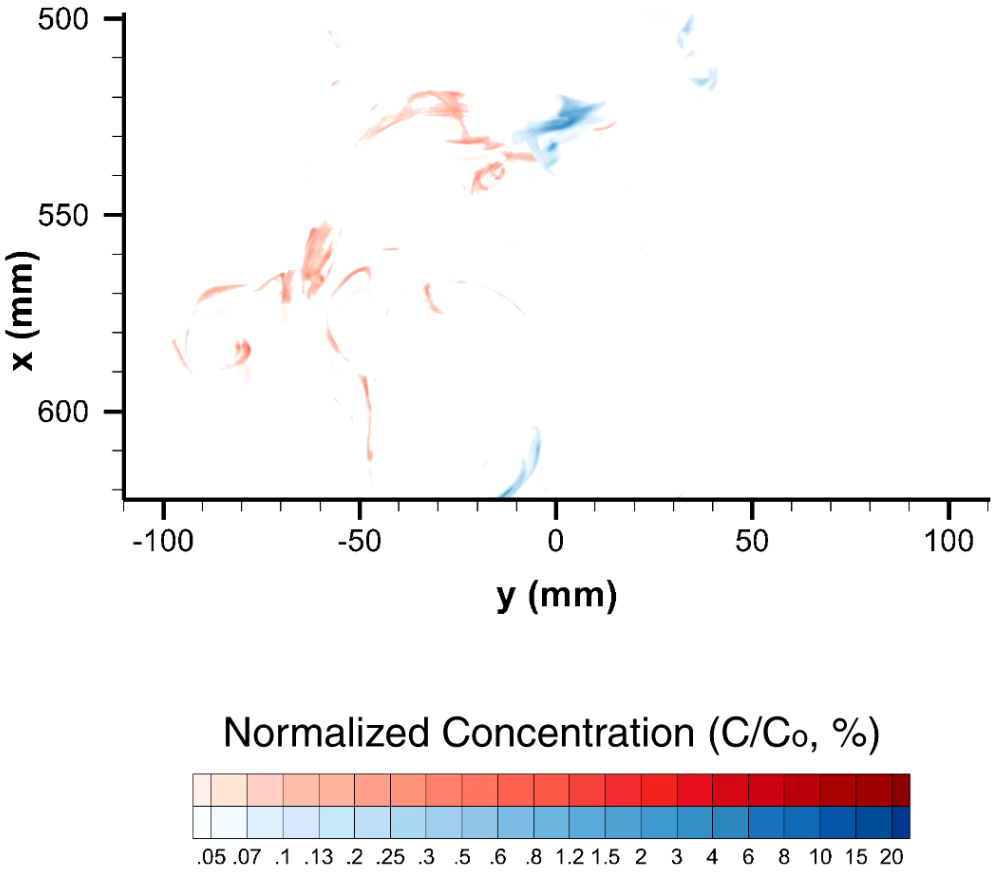

6

Figure 5.14: Example of simultaneously-collected concentration fields that show the interaction between the rhodamine 6G and oxazine 725 dye plumes (at 88.1 seconds).

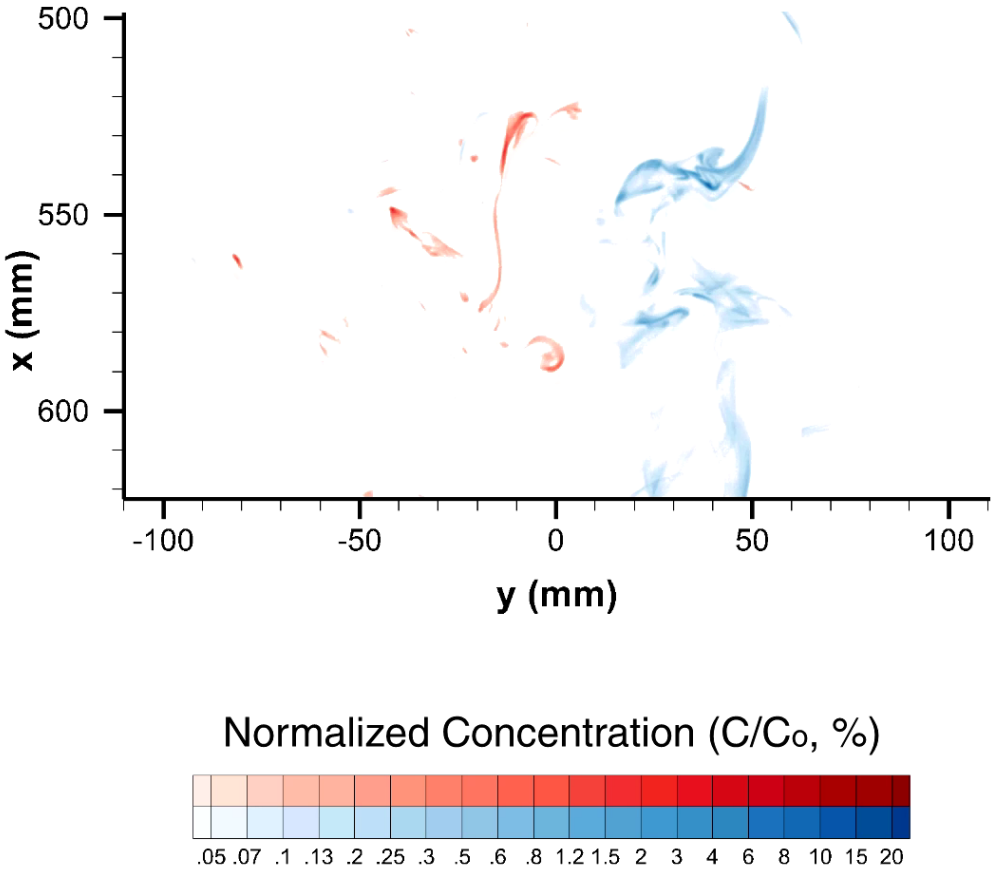

Figure 5.15: Example of simultaneously-collected concentration fields that show the interaction between the rhodamine 6G and oxazine 725 dye plumes (at 49.1 seconds).

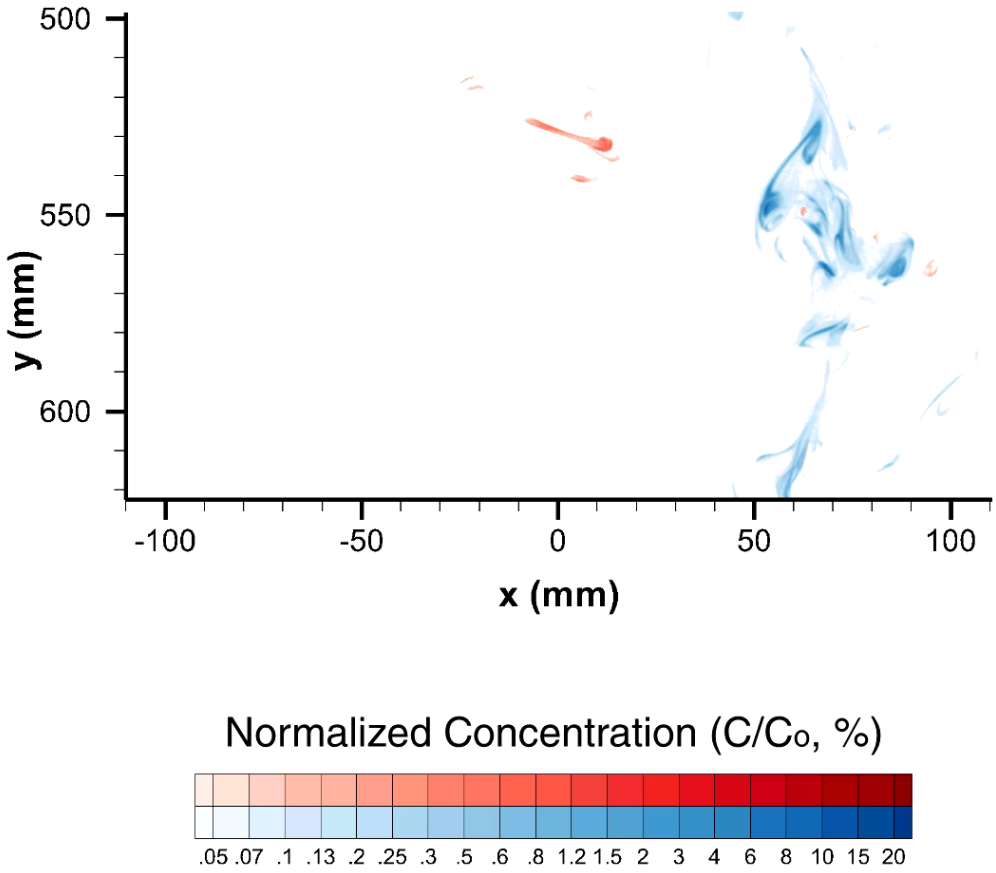

Figure 5.16: Example of simultaneously-collected concentration fields that show the interaction between the rhodamine 6G and oxazine 725 dye plumes (at 98.0 seconds).

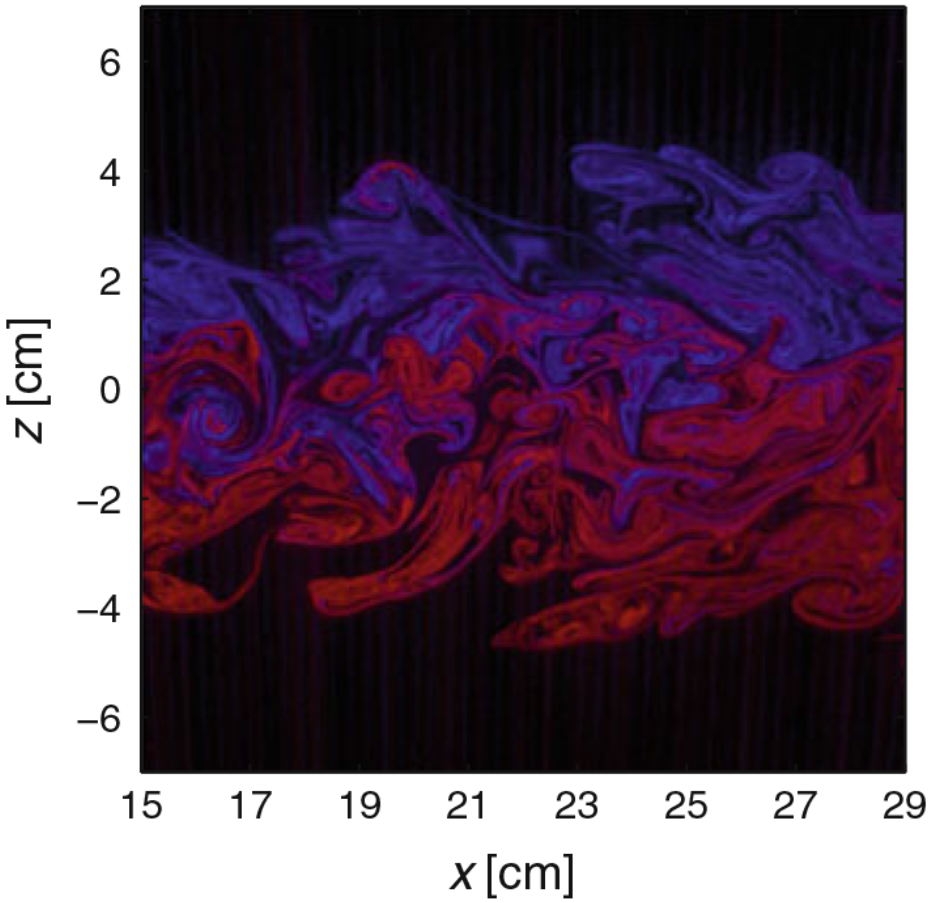

Figure 5.17: Composite image of an x-z slice through the fluorescein and oxazine 725 concentration fields showing interaction between the two jets (Soltys and Crimaldi 2010).

consistent with the results of Soltys and Crimaldi (2010). If Figure 5.17 is compared to our two-color PLIF results, striking similarities are observed. It is very clear that there is overlap and mixing occurring between the fluorescein and oxazine 725 jets. Again, intrusion seems to favor regions that do not already contain dye. However, overlap and mixing is more predominant compared to our results due to jets releasing dye at 20.2 cm/s into a 1 cm/s ambient flow, resulting in higher turbulence and mixing.

CHAPTER VI

CONCLUSION

A planar laser induced fluorescence (PLIF) technique was employed to measure the concentration of dye in a rhodamine 6G and salt solution over an area roughly the same size as a conductivity probe sensor located 0.5 meters downstream from the dye/salt iso-kinetic release and 1 cm upstream of the conductivity probe. The two methods of concentration measurement (i.e. PLIF and probe) were used to capture sets of synchronized data at a frequency of 10 Hz. The PLIF image intensity was converted to concentration using a linear relationship between intensity and dye concentration calculated from calibration images. Absorption, attenuation of the laser light, and spatial mapping and calibration were corrected for before averaging and converting intensity to concentration over the area of interest. Conductivity probe voltage readings were converted to salt concentration values using a linear calibration relationship. Both data sets of concentrations were converted to concentrations normalized by the dye/salt source values, respectively, and expressed as percentages. The 1 cm separation distance between the probe and averaging area in the PLIF image was corrected for using the mean flow velocity so that the two different data sets could be directly compared.

The majority of the comparable normalized concentration pairs in the first experiment did not match well, although for several of the concentration spikes in either data set there was a matching spike of a different value in the other data set. The conductivity probe data seemed to miss more spikes in concentration when compared with the PLIF concentration spikes (this is more obvious by referring to Figure 5.2). These characteristics are a direct result of mostly uncorrelated data. This lack of

correlation directly resulted from a combination of separation distance between PLIF averaging area and conductivity probe tip. It was found that the separation distance of 1 cm between the PLIF averaging area and the probe sensor tip was a major cause of the discrepancy between the two data sets. Utilizing instantaneous velocity measurements of the flume flow velocity at every time step, the averaging area could have been varied very slightly in the streamwise direction to obtain a more accurate comparison. Additionally, due to turbulence, the planar concentration field may also have missed certain areas of filaments as they moved up or down in the z (vertical) direction out of the plane that the camera was imaging (the same plane as the conductivity probe tip). Additionally, the dye/salt plume was stretching and changing size and shape slightly even in a single time step, which affected whether or not a part of a filament would have been in the averaging area. Had the averaging area been much closer to the probe sensor tip, the results would have been much closer to one another and have a higher correlation. Unfortunately, this was not possible mainly due to the plastic shielding of the conductivity probe protecting the sensor. Therefore, determining the accuracy of conductivity probes used to instantaneously measure concentration was not achieved with high precision with the current set up. The only way to properly compare the two different sampling methods would be to utilize long time series of data (over five minutes) to calculate proper statistics such as mean concentration and standard deviation to compare with one another. However, the constraints of the experiment prevent utilization of lengthy time series and such statistics. Alternatively, it was possible for the shielding to be removed and this would have solved the separation distance issue as well as the effects on the flow due to the shielding itself.

A two-color PLIF technique was used to study the interaction between two different dye plumes of rhodamine 6G and oxazine 725 released 10 cm apart (transverse direction) iso-kinetically to a surrounding flow with a mean velocity of 5 cm/s. Two

cameras were positioned and calibrated to have their fields of view spatially correspond to the same physical location. Similar calibration methods to the single-color PLIF were used for each of the two different dyes and the same corrections were made to every image. These image sets were converted to spatial coordinates and concentration values at each pixel of every image then superimposed to create a single figure of the overlapping plume structures. 3000 images were captured through each camera but only the first half were used in analysis for a total time series of 150 seconds or 2.5 minutes.

The most important result of the two-color PLIF measurements was the "proof-of-concept" for the dual measurement technique. While the method builds on previous designs, our system is particularly focused on the dual plume application. The two-color PLIF results reveal several areas of interaction between the two concentration fields. This interaction is due to turbulent stirring and molecular diffusion acting across both plumes and results in several small regions of overlap. When filaments from the two plumes overlap, the turbulent stirring and molecular diffusion processes begin to mix the regions of overlap. This mixing is expected to further homogenize those regions farther downstream.

Chemosensory cues obtained from two plumes with interaction are very similar to plumes with no interaction, which is expected since the chemical is considered a passive tracer. At a short distance downstream, as is the case in our streamwise location of study, two plumes had begun to show signs of mixing. If a blue crab was to be presented with this information, it should need to weigh the advantage of tracking an attractive odorant in the presence of an aversive odorant. Greater interaction between plumes further downstream may confuse the animal or at least present it with more conflicting cues. Further study with different effluent release configurations together with animal behavior observations at different downstream locations would be of great interest in determining the overlap of the plume structures

and the resulting influence on tracking behavior.

APPENDIX A

```
clc
clearvars
avg=[];
for i=1:499
    dd=0;
    ddd=0;
    h=[];
    d=[];
    if i<10
        path=['B0000' num2str(i) '.dat'];
    elseif i<100
        path=['B000' num2str(i) '.dat'];
    else
        path=['B00' num2str(i) '.dat'];
    end
    [h,d]=hdrload(path);
    for j=1:size(d,1)
        if (d(j,1)>-0.5 && d(j,1)<0.5) && (d(j,2)>0.00 && d(j,2)<0.25)
            dd=dd+1;
            ddd=ddd+d(j,3);
        end
    end
    avg(i)=ddd/dd;
end
a=transpose(avg);
save avg.txt a -ASCII
```

Figure A.1: MATLAB code used to average the total concentration found in a $0.05mm^2$ rectangular area over the area at the bottom-center of each of 500 images.

REFERENCES

[1] A. J. Ferrier, D. R. Funk, P. J. W. R., "Application of optical techniques to the study of plumes in stratified fluids," *Dynamics of Atmospheres and Oceans*, vol. 20, pp. 155–183, 1993.

[2] B. D. Dickman, D. R. Webster, J. L. P. M. J. W., "Three-dimensional odorant concentration measurements around actively tracking blue crabs," *Limnology and Oceanography: Methods*, vol. 7, pp. 96–108, 2009.

[3] Crimaldi, J. P., "The effect of photobleaching and velicity fluctuations on single-point lif measurements," *Experiments in Fluids*, vol. 23, pp. 325–330, 1997.

[4] Crimaldi, J. P., "Planar laser induced fluorescence in aqueous flows," *Experiments in Fluids*, vol. 44, pp. 851–863, 2008.

[5] Crimaldi, J. P. and Koseff, J. R., "High-resolution measurements of the spatial and temporal scalar structure of a turbulent plume," *Experiments in Fluids*, vol. 31, pp. 90–102, 2001.

[6] Crimaldi, J. P. and Koseff, J. R., "Structure of turbulent plumes from a momentumless source in a smooth bed," *Environ Fluid Mech*, vol. 6, pp. 573–592, 2006.

[7] D. R. Webster, S. Rahman, L. P. D., "On the usefulness of bilateral comparison to tracking turbulent chemical odor plumes," *Limnol. Oceanogr.*, vol. 46, pp. 1048–1053, Mar. 2001b.

[8] D. R. Webster, K. Y. Volyanskyy, M. J. W., "Bioinspired algorithm for autonomous sensor-driven guidance in turbulent chemical plumes," *Bioinspiration and Biomimetics*, 2012.

[9] D. S. Nichols, C. H. Brown, C. F. D., "Laser-induced fluorescence as a method for measuring mass-transfer rates and for flow visualization," *Bulletin Of The American Physical Society*, vol. 17, no. 11, p. 1091, 1972.

[10] Dahm, W. J. A. and Dimotakis, P. E., "Measurements of entrainment and mixing in turbulent jets," *AIAA Journal*, vol. 25, no. 9, pp. 1216–1223, 1987.

[11] Dasi, L. P., *Statistical Characteristics of Turbulent Chemical Plumes*. M.S. Thesis, Georgia Institute of Technology, 2000.

[12] Fackrell, J. E. and Robins, A. G., "Concentration fluctuations and fluxes in plumes from point sources in a turbulent boundary layer," *J. Fluid Mech.*, vol. 117, pp. 1–26, 1982.

[13] J. L. Jackson, D. R. Webster, S. R. M. J. W., "Bed-roughness effects on boundary-layer turbulence and consequences for odor-tracking behavoir of blue crabs," *Limnol. Oceanogr.*, vol. 52, no. 5, pp. 1883–1897, 2007.

[14] J. P. Crimaldi, M. B. Wiley, J. R. K., "The relationship between mean and instantaneous structure in turbulent passive scalar plumes," *Journal of Turbulence*, vol. 3, 2002.

[15] Koochesfahani, M. M. and Dimotakis, P. E., "Laser-induced fluorescence measurements of mixed fluid concentration in a liquid plane shear layer," *AIAA Journal*, vol. 23, pp. 1700–1707, Nov. 1985.

[16] Liu, K. and Parson, J. M., "Laser fluorescence detection of nascent product state distributions in reactions of sc and y with o-2, no, and so2," *Journal of Chemical Physics*, vol. 67, no. 5, pp. 1814–1828, 1977.

[17] M. J. Weissburg, D. B. Dusenbery, H. I. J. J. T. K. P. J. R. D. R. W., "A multidisciplinary study of spatial and temporal scales containing information in turbulent chemical plume tracking," *Environmental Fluid Mechanics*, vol. 2, pp. 65–94, 2002.

[18] Melton, L. A. and Lipp, C. W., "Criteria for quantitative plif experiments using high-power lasers," *Experiments in Fluids*, vol. 35, pp. 310–316, 2003.

[19] Natrajan, V. K. and Christensen, K. T., "Two-color laser-induced fluorescent thermometry for microfluidic systems," *Measurement Science and Technology*, vol. 20, 2008.

[20] Owen, F. K., "Laser velocimeter measurements of structure of turbulent spray flames," *Astronautics & Aeronautics*, vol. 15, no. 10, p. B19, 1977.

[21] Rahman, S. and Webster, D. R., "The effect of bed roughness on scalar fluctuations in turbulent boundary layers," *Experiments in Fluids*, vol. 38, pp. 372–384, 2005.

[22] Soltys, M. A. and Crimaldi, J. P., "Scalar interactions between parallel jets measured using a two-channel plif technique," *Experiments in Fluids*, Dec. 2010.

[23] Tokumaru, P. T. and Dimotakis, P. E., "Image correlation velocimetry," *Experiments in Fluids*, vol. 19, pp. 1–15, 1995.

[24] Walker, D. A., "A fluorescence technique for measurement of concentration in mixing liquids," *Journal of Physics E: Scientific Instruments*, vol. 20, pp. 217–224, 1987.

[25] Webster, D. R. and Weissburg, M. J., "Chemosensory guidance cues in a turbulent chemical odor plume," *Limnol. Oceanogr.*, vol. 46, no. 5, pp. 1034–1047, 2001a.

[26] Weissburg, M. J. and Zimmer-Faust, R. K., "Odor plumes and how blue crabs use them in finding prey," *Journal of Experimental Biology*, vol. 197, pp. 349–375, 1994.

[27] Y. Watanabe, Y. Hashizume, N. F., "Temperature measurement by two-color lif technique using nd:yag lasers," *Journal of Visualization*, vol. 10, no. 4, pp. 343–344, 2007.